NATIONAL AERONAUTICS AND SPACE ADMINISTRATION

Technical Memorandum 33-690

Development and Correlation: Viking Orbiter Analytical Dynamic Model With Modal Test

B. K. Wada, J. A. Garba, and
J. C. Chen

PRICES SUBJECT TO CHANGE

JET PROPULSION LABORATORY
CALIFORNIA INSTITUTE OF TECHNOLOGY
PASADENA, CALIFORNIA

June 1, 1974

46

Prepared Under Contract No. NAS 7-100
National Aeronautics and Space Administration

PREFACE

The work described in this report was performed by the Applied Mechanics Division of the Jet Propulsion Laboratory.

CONTENTS

Introduction 1

Description of Hardware 2

General Approach 4

A. Load Analysis and Its Impact 4

B. Member Loads 5

C. Substructure Modal Coupling 5

D. Rigid VLC 5

Analysis 5

A. Substructures 6

B. Displacement Functions of Substructures 6

C. Rigid Body Modes 6

D. Constraint Modes 7

E. Attachment Modes (Ref. 5) 7

F. Normal Modes 7

G. Total Displacement Function 7

H. Generalized Coordinates 7

I. Mixed Coordinates 8

J. Equation of Motion of Total Structure 8

K. Size of the Problem 10

Substructure Tests and Analysis Correlation 10

A. Propulsion Module Modal Test 10

B. Solar Panel Modal Test 11

System Modal Test and Analysis Correlation 11

A. Modal Test Configuration 11

B. Correlation 15

C. Mode Identification 16

CONTENTS (contd)

D. Modal Test Equation 17

E. Modal Test Output 18

F. Frequency 18

G. Orthogonality 18

H. Effective Mass 18

I. Mode Shape 21

J. Local Kinetic Energy 25

K. Modal Force 26

L. Strain Energy 31

M. Reaction Forces 34

N. Generalized Mass From Modal Damping 34

Final Dynamic Model 37

Conclusion 39

References 39

TABLES

1. Approximate Weights 3

2. Approximate Propellant Weight and Ullage Summary 3

3. Size of VO Dynamic Model 10

4. Frequency Change and Damping of Propulsion Subsystem Modal Test 12

5. Kinetic Energy Distribution of Propulsion Module Modal Test 13

6. Modal Forces of Subsystem Modal Test 14

7. Frequency Change and Damping of Solar Panel Modal Test 15

8. Mixed Orthogonality – Model VIII 16

9. Cross-Orthogonality – Orthogonality of Test Mode No. 701; Run Name DTA701 at Frequency 7.84 Hz with Respect to all Analytical Modes 17

CONTENTS (contd)

10.	Modal Frequency Comparison	19
11.	Orthogonality	19
12.	Effective Mass in Percentage	20
13.	Modal Comparison – Analytical Mode 3 vs Experimental Mode 701	22
14.	Summary of Mode Shape Comparison	24
15.	Kinetic Energy Comparison – Analytical Mode 3 vs Test Mode 701	25
16.	Summary of Kinetic Energy Comparison	27
17.	Axial Force Comparison – Factor = 6.076	28
18.	Modal Force Comparison Errors	30
19.	Composite Error of VLCA and V-S/C-A	31
20.	Comparison of Modal Force by Inertia Load – Mode 713, Frequency 26.49 Hz	31
21.	Strain Energy Comparison – Analytical Mode vs Test Mode 701	32
22.	Strain Energy in Order of Magnitude – Analytical Mode 3 vs Test Mode 701	33
23.	Strain Energy Distribution Comparison	35
24.	Comparison of Reaction Force	36
25.	Generalized Mass Comparison	37
26.	Test Verified Models	38

DEVELOPMENT AND CORRELATION: VIKING ORBITER ANALYTICAL DYNAMIC MODEL WITH MODAL TEST*

B. K. Wada, J. A. Garba, and J. C. Chen
Jet Propulsion Laboratory
Pasadena, California

The Jet Propulsion Laboratory is responsible for the Viking Orbiter System, which is part of the overall Viking Project managed by the Viking Project Office at Langley Research Center for NASA.

The development of a mathematical dynamic model and its verification by a modal test is a significant milestone for many Projects including Viking Orbiter (VO). Difficulties encountered include performing a modal test, establishing a criteria for correlation of analysis with test, and modifying a large finite element mathematical model to match test data if required. Often the modal test is performed near the end of the Project development schedule; consequently, the time alloted to obtain a verified mathematical model is minimal.

The paper describes the VO experience in the achievement of a good mathematical model. Success can be attributed to the coordination of analysis and tests using substructure modal coupling techniques. The experience would benefit the overall planning of any project, such as Shuttle, especially if substructure modal coupling techniques are contemplated.

INTRODUCTION

The Jet Propulsion Laboratory (JPL) is responsible for the Viking Orbiter System, which is part of the overall Viking Project managed by the Viking Project Office at Langley Research Center (LRC) for NASA. The Spacecraft will be launched on a Titan IIIE/ Centaur Launch Vehicle in August 1975.

The total launch vehicle system consists of numerous subsystems that are developed by various aerospace organizations. The creation of a launch vehicle system model requires the transfer of each organization's mathematical models. One organization eventually creates the total model required for analyses. The complexity and size of the problem required the use of substructure modal coupling concepts. To minimize schedule and cost, the goal was to limit the responsibilities of each organization to their own mathematical models and verification test program. A strong emphasis on technical accuracy existed.

The development of a test-verified mathematical dynamic model is a significant milestone for many projects including Viking Orbiter (VO). Difficulties encountered include performing a modal test, establishing a criterion for correlation of analyses with the test, and modifying a large finite element mathematical model to match test data if required. Since the modal test was performed near the end of the Project development schedule, the time available to obtain a test-verified mathematical dynamic modal was minimal. This paper describes the VO plans and experience to

obtain a good model. Emphasis was placed on the early development of good mathematical models, performance of the modal test, and methods to correlate the analysis with test data.

A valid mathematical model for VO was required because the design and flight loads for the primary structure were established by load analysis. Load analysis is a procedure for obtaining VO member forces from the dynamic response of a complex finite element model of the complete Launch Vehicle System (including the VO) subjected to launch vehicle engine transients. Load analysis requires substructure modal coupling (Ref. 1) of the various structural subsystems of the Launch Vehicle System to allow a solution within present computer capabilities. In addition to the usual objectives of modal tests, determination of individual member forces is emphasized throughout the program.

A good mathematical model was generated by establishing an overall plan integrating subsystem analysis and test with the substructure modal coupling approach. Thus the model was continually updated during the program.

Emphasis was also placed on the modal test and the establishment of a measure of correlation of the analysis with the test. The measure of correlation is required to establish a factor directly related to the confidence placed in the member forces resulting from load analysis.

This paper describes three general activities that resulted in the VO analytical dynamic model, and that were updated and verified by test data during the Project.

(1) The generation of the overall plan for load analysis, an analytical dynamic model, and development tests.

(2) The performance of VO subsystem static and modal tests.

(3) The correlation of the VO System modal analysis and test.

The details of the modal test are not included (Ref. 2). However, actual results are used to show the degree of success attained on a large complex structure. The substructure, tests, and update of substructure mathematical models occurred between July 1, 1972 and May 15, 1973, and the VO System modal test between June 1, 1973 and July 30, 1973. The correlation of modal test results with analysis occurred between July 1, 1973 and July 30, 1973. The final mathematical model was completed on schedule by July 30, 1973.

DESCRIPTION OF HARDWARE

Figure 1 identifies parts of the Viking spacecraft (V-S/C), Viking transition adapter (VTA), and Centaur truss adapter (CTA) pertinent to this discussion.

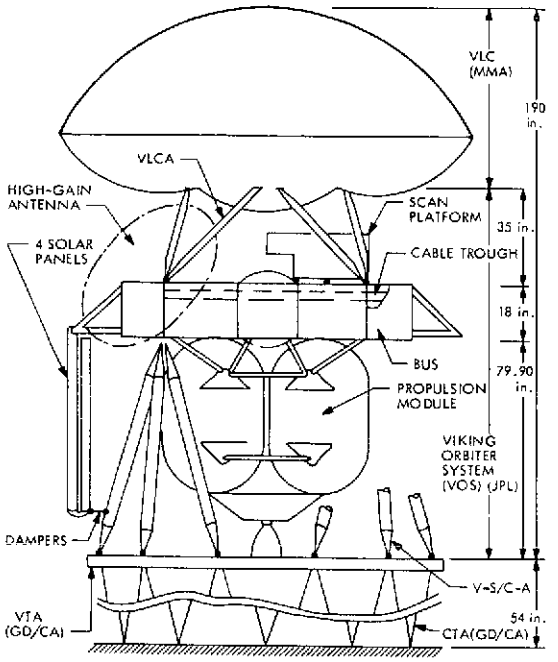

Fig. 1 - Viking spacecraft

The Viking Orbiter System was complicated because it is situated between the Viking lander capsule (VLC) on top and the Centaur adapter (VTA/CTA) on the bottom. The VLC and the VTA/CTA are the responsibility of Martin Marietta Aerospace (MMA) and General Dynamics/Convair Astronautics (GD/CA) respectively.

The weight of the hardware is summarized in Table 1.

Figure 2 is a description of the VO/VTA/CTA configuration for the modal test performed at JPL.

Figure 3 is a photograph of the test of the orbiter development test model (ODTM). The rationale of the configuration will be discussed. The major differences between the test and

TABLE 1
Approximate Weights*

Hardware	Weight (lb)	Responsible Organization
VLC	2567	MMA
VOS		JPL
Bus and adapters	1109	
High-gain antenna with support	47	
Scan platform with support	201	
Four solar panels	244	
Cable trough	49	
Propulsion module hardware	512	
Propellants*†	3138	
VTA	‡	GD/CA
CTA	‡	GD/CA
Total weight	7867	LRC

*The weights are the values used for analysis on 7/1/73.
†See Table 2.
‡Included in the Centaur Model.

TABLE 2
Approximate Propellant Weight and Ullage Summary

Configuration	Oxidizer				Fuel			
	Fluid	Rigid Weight (lb)	Slosh Weight (lb)	Ullage (%)	Fluid	Rigid Weight (lb)	Slosh Weight (lb)	Ullage (%)
Viking Mission A1	N_2O_4	1379	431	20.9	MMH*	968	235	13.3
Viking Mission A2	N_2O_4	1318	428	23.7	MMH	911	249	16.36
Viking Mission B	N_2O_4	1470	415	17.62	MMH	1049	204	9.68
Modal test	Freon-TF	1735	371	17.62	Alcohol	902	227	9.68

*Monomethyl hydrazine.

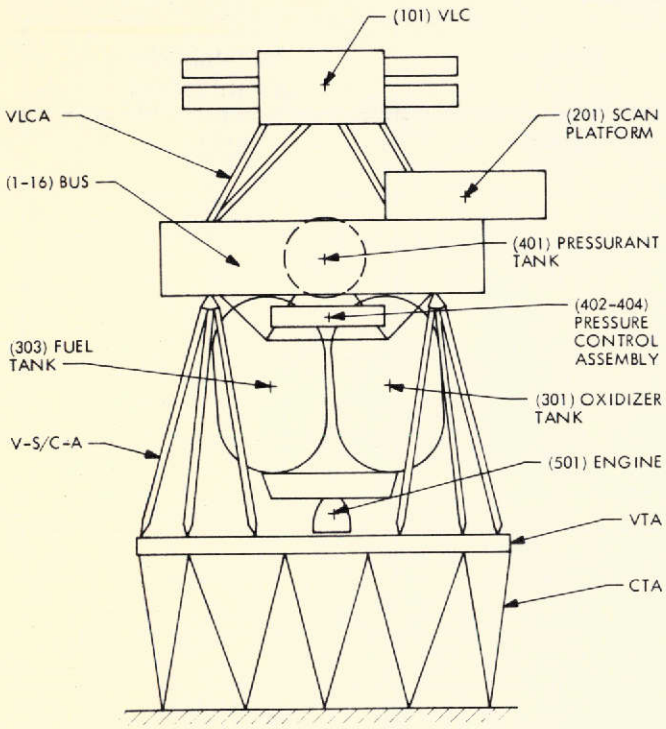

Fig. 2 - Test configuration and node identification

flight configurations are that the test configuration has:

(1) Rigid VLC with inertia property simulation.

(2) No solar panels and solar panel dampers.

(3) No high gain antenna.

(4) Propulsion propellant mass loading as shown in Table 2.

(5) Mass and stiffness to represent dynamic characteristics up to 60 Hz.

(6) No slippage of the scan platform joint along the serrations.

The propellant loading for different configurations is summarized in Table 2. The information will be of value for future discussion.

GENERAL APPROACH

The analysis plan and modal test approach were closely integrated with VO Project plans and requirements (Ref. 3). Our belief is that a successful development of a mathematical model correlated by test is directly related to the overall analysis, hardware, and test plan.

A. Load Analysis and Its Impact

The design and flight loads for the primary structural members were established by load analysis. The load analysis is a dynamic analysis procedure to obtain VO member forces. The complete Launch Vehicle System including the VO is subjected to launch vehicle engine transients measured from past flights.

The use of load analysis for design and flight loads necessitated a continual reiteration of the VO mathematical model to update the design loads as the design evolved. A VO model of the final configuration verified by a

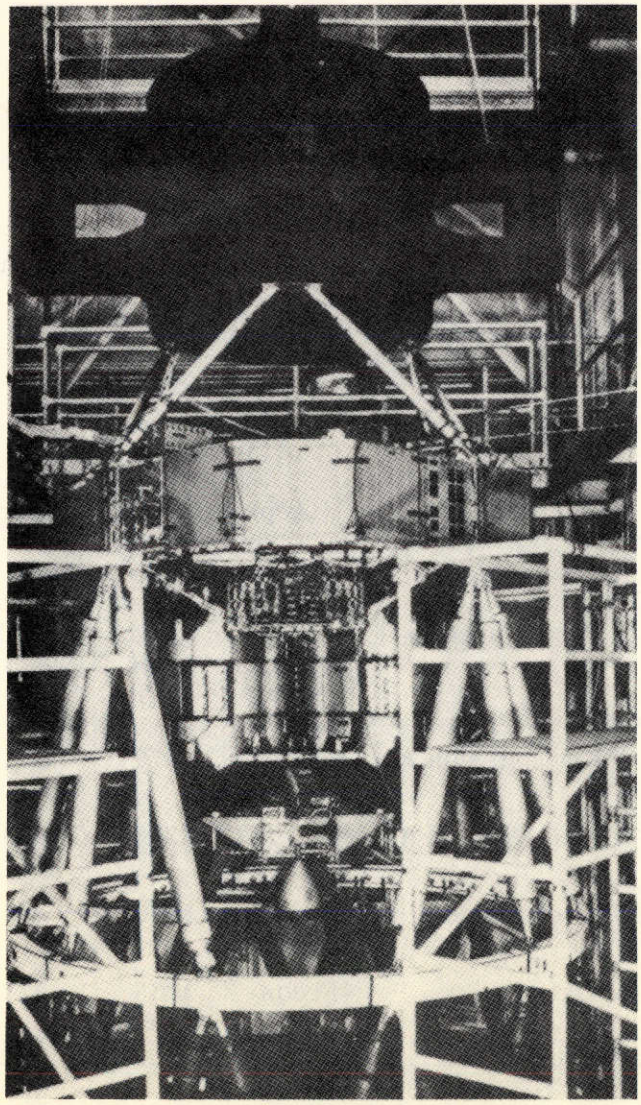

Fig. 3 - ODTM modal test

system test was required. The flight loads were used to establish forces for which the structure was qualified.

The establishment of flight loads and the structural qualification test program were near the end of the development schedule. Since the modal test was also near the end of the development schedule, confidence had to exist in the mathematical model when the modal test was performed.

Correlation of the modal test results to analysis was necessary to help establish a measure of uncertainty, which was required to establish the accuracy of flight loads. The measure of uncertainty is defined as the load analysis factor (LAF). The flight loads are the calculated loads times the LAF.

B. Member Loads

The significant parameter in load analysis is the member forces. The goal was to obtain accurate dynamic member forces, not accelerations. The modal test included the measurement of modal force coefficients.

C. Substructure Modal Coupling

The modal coupling of the VO with the VLC and VTA/CTA required consideration of:

(1) Accurate selection of displacement functions.

(2) Simplification of interfaces between organizations.

(3) Provision for each organization to perform analyses and tests independent of the others.

(4) Ability to verify the model by modal test.

(5) Availability of test hardware.

The structure below the CTA was modeled as a planar structure (plane before deformation remains a plane after deformation) and the structure above the VTA was a three-dimensional model. The requirement to modally couple the V-S/C to the Centaur resulted in the decision to include the VTA/CTA with the VO. Otherwise, the number of compatibility relationships would have increased along with the possibility of erroneous data caused by round-off errors. Consequently, the CTA/VTA was included as a part of the VO modal test. Another goal was to simulate the interfaces since truss joints were of concern.

The substructure modal coupling analysis techniques were also used on VO to:

(1) Provide a cost effective solution.

(2) Allow use of substructure test data as available.

(3) Decrease the effort to update the mathematical model based on the test data.

(4) Increase confidence in the final model.

A substructure was defined as being compatible with:

(1) Deliverable hardware used to obtain test data incorporable into the models.

(2) Ease of interface definition and analysis.

(3) Area of engineering responsibility.

Substructure tests were used to verify and adjust the mathematical models. Errors were minimized since the responsible engineer of a substructure used engineering judgement to verify his mathematical model.

D. Rigid VLC

Various methods of modal coupling of the VO to the VLC were possible. The inclusion of the rigid VLC is mathematically equivalent to mass loading (Ref. 4) the VO interface with the VLC. The disadvantage of including VLC data into the VO analysis and test were offset by:

(1) The capability to modify the rigid VLC inertia properties after the VO model was delivered to MMA.

(2) The similarity of the VO displacement functions to V-S/C functions, thus fewer modes were required.

(3) The capability to use the resulting representative configuration for the sine vibration tests.

ANALYSIS

The equations are developed to briefly illustrate the methodology in the creation of the

VO mathematical model. Also they are used as a basis to definitize the objectives of the tests and to define the data used to correlate the analyses with test data.

A. Substructures

The two general equations for the substructure are:

$$\begin{bmatrix} k_{II} & k_{IO} \\ k_{OI} & k_{OO} \end{bmatrix} \begin{Bmatrix} U_I \\ U_O \end{Bmatrix} = \begin{Bmatrix} f_I \\ f_O \end{Bmatrix} \text{ or } [k]\{u\} = \{f\} \quad (1)$$

$$[m]\{\ddot{u}\} + [c]\{\dot{u}\} + [k]\{u\} = \{0\} \quad (2)$$

$$\{P\} = [S]\{u\} \quad (3)$$

where

$[k]$ = stiffness matrix

$[c]$ = damping matrix

$[m]$ = mass matrix

$[f]$ = force matrix

$\{P\}$ = member forces

$[S]$ = force coefficient matrix

$\{u\}$ = displacement

I = subscript representing interface degree of freedom

O = subscript representing degree of freedom other than the interface

Equation (2) can be derived from the Lagrangian equation:

$$\frac{d}{dt}\left(\frac{\partial L}{\partial \dot{u}_j}\right) - \frac{\partial L}{\partial u_j} + \frac{\partial D}{\partial \dot{u}_j} = F_j \quad (4)$$

where

$$L = T - U$$

$$T = \frac{1}{2}\{\dot{u}\}^T [m]\{\dot{u}\} = \frac{1}{2}\sum_{j=1}^{N} \{\dot{u}\}_j^T [m]_j \{\dot{u}\}_j$$

$$U = \frac{1}{2}\{u\}^T [k]\{u\} = \frac{1}{2}\sum_{j=1}^{N} \{u\}_j^T [k]_j \{u\}_j$$

$$D = \frac{1}{2}\{\dot{u}\}^T [c]\{\dot{u}\} = \frac{1}{2}\sum_{j=1}^{N} \{\dot{u}\}_j^T [c]_j \{\dot{u}\}_j \quad (5)$$

F_j = force

N = number of finite elements

$\{u\}_j, \{\dot{u}\}_j, [m]_j, [k]_j$ = parameters associated with the j^{th} finite element.

Other parameters for correlation of the analysis and test data are the kinetic energy T and the potential energy U. The dissipation function D cannot be used for correlation since the test data are used in the analysis. Equation (1) can be written as:

$$[u_O] = [k_{OO}]^{-1}\left([f_O] - [k_{OI}][u_I]\right) \quad (6)$$

and Eq. (2) as:

$$[m]\{\ddot{u}\} + [k]\{u\} = \{0\} \quad (7)$$

where experimental modal damping values are used. The $[c]$ is assumed to be of a form where the transformation formed by the eigenvectors of Eq. (7) uncouples Eq. (2).

B. Displacement Functions of Substructures

Often the dynamic characteristics of substructures are represented by a finite number of displacement functions to reduce the number of independent variables. The various forms of identification of displacement functions will be discussed.

C. Rigid Body Modes

Rigid body modes represent the motions $[\phi_R]$ of the substructure when a degree-of-freedom $[u_I]$ is displaced an arbitrary value without force. The $[\phi_R]$ is a solution to Eq. (6), where $[f_O] = 0$, $[u_I]$ is a unit matrix in the degrees of freedom associated with the

rigid body modes. The displacements of the substructure due to rigid body modes are

$$\{u_R\} = [\phi_R]\{q_R\} \tag{8}$$

The number of rigid body motions may range from 1 to ∞. Rigid body motions in excess of 6 are related to linkages within the substructure.

If the displacement at the substructure interface gridpoints can be represented by a linear combination of rigid body modes, the interface is defined as statically determinant.

D. Constraint Modes (Ref. 1)

Constraint modes represent the motions $[\phi_C]$ of the substructure when the displacement of an interface degree of freedom (DOF) requires force as the other interface degrees of freedom are restrained. Constraint modes are used to define displacement functions corresponding to interface distortions. The constraint modes $[\phi_C]$ are the solution to Eq. (6), where $[f_O] = 0$, $[u_I]$ is a unit matrix in the degrees of freedom associated with constraint modes. A force matrix $[f_C]$ associated with constraint modes exists. Note that a distinction between rigid body modes and constraint modes is not required. The displacements of the substructure due to constraint modes are

$$\{u_C\} = [\phi_C]\{q_C\} \tag{9}$$

They are defined only if the interfaces are statically indeterminant. (Interface cannot be defined as a linear combination of rigid body modes.)

Features of constraint modes include orthogonal to normal modes evaluated with all interface degrees of freedom constrained.

E. Attachment Modes (Ref. 5)

The number of displacement functions necessary to represent the dynamic characteristics of the system may be minimized by the selection of substructure modes that closely represent system modes. In a combined structural system, a gridpoint of a substructure at which another substructure is attached is subjected to concentrated attachment forces. These forces result in a displacement function that may have to be represented by many normal modes.

Attachment modes are displacements $[\phi_A]$ of the substructure corresponding to concentrated loads $[f_A]$ on the substructure. Displacement $[\phi_A]$ are the solution to Eq. (6), where $[f_O] = [f_A]$ and $[u_I] = 0$. The displacements due to attachment modes are

$$\{u_A\} = [\phi_A]\{q_A\} \tag{10}$$

A disadvantage of attachment modes is nonorthogonality to the normal modes or to each other. Thus, unless extreme care is exercised, attachment modes that are nearly linear combinations of normal modes or other attachment modes may inadvertently be selected. If the system equations comprising substructure modes are not independent, the equations cannot be solved.

F. Normal Modes

The normal modes of the substructure are evaluated from Eq. (7). The displacements due to normal modes are

$$\{u_N\} = [\phi_N]\{q_N\} \tag{11}$$

G. Total Displacement Function

The displacement of the substructure can be any combination of displacement functions selected above.

$$\{u\} = \left[[\phi_R][\phi_C][\phi_A][\phi_N]\right]\begin{Bmatrix} q_R \\ q_C \\ q_A \\ q_N \end{Bmatrix} = [\phi]\{q\} \tag{12}$$

H. Generalized Coordinates

Substitution of Eq. (12) into Eq. (7) and premultiplication by $[\phi]^T$ result in

$$[\phi]^T[m][\phi]\{\ddot{q}\} + [\phi]^T[k][\phi]\{q\} = \{0\}$$

or

$$\begin{aligned} [m_q]\{\ddot{q}\} + [k_q]\{q\} &= \{0\} \\ [S][\phi]\{q\} &= \{P\} \end{aligned} \tag{13}$$

Damping corresponding to the displacement functions is introduced into Eq. (2) if desired.

$$\left[m_q\right]\left\{\ddot{q}\right\}+\left[c_q\right]\left\{\dot{q}\right\}+\left[k_q\right]\left\{q\right\}=\left\{0\right\} \quad (14)$$

I. Mixed Coordinates

Equation (14) represents the equation of motion of any substructure in terms of its generalized coordinates. The VO analysis approach uses hybrid coordinates where the real displacements of the bus are retained and the generalized coordinates of the substructure attached to the bus are used.

Mixed coordinates were used because of the order of the system equations of motion. Originally generalized coordinates for all subsystems were retained as described in Ref. 6. This approach resulted in numerical difficulties due to limitations of single precision arithmetic in the Structural Analysis and Matrix Interpretive System (SAMIS) on the Univac 1108 computer. The use of real coordinates for all subsystems was rejected because of size limitations in the eigenvalue routine. The symbols used are shown below.

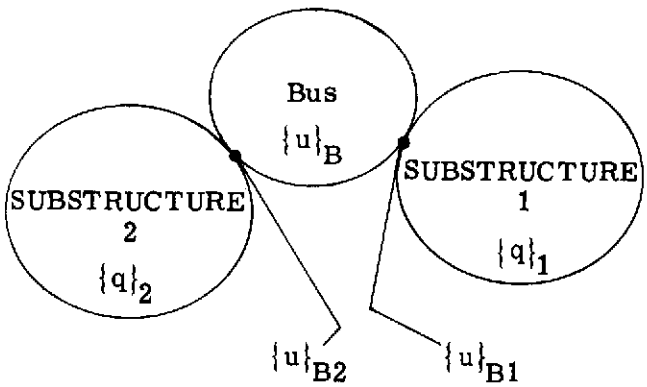

The terms are defined. Subscripts differentiating substructures are introduced at this time.

$\{q\}_i$ = generalized coordinates of i^{th} substructure

$\{u\}_B$ = real displacement of the VO bus

$\{u\}_{Bi}$ = subset of $\{u\}_B$ defining compatibility of the i^{th} substructure to the bus. Often the displacements are in local coordinates.

The Eq. (14) for the i^{th} substructure with the interface degrees of freedom is

$$\left[m_q\right]_i\begin{Bmatrix}\{\ddot{u}\}_{Bi}\\ \{\ddot{q}\}_i\end{Bmatrix}+\left[c_q\right]_i\begin{Bmatrix}\{\dot{u}\}_{Bi}\\ \{\dot{q}\}_i\end{Bmatrix}$$

$$+\left[k_q\right]_i\begin{Bmatrix}\{u\}_{Bi}\\ \{q\}_i\end{Bmatrix}=\left\{0\right\} \quad (15)$$

Two classes of interfaces are distinguished. Statically determinant and statically indeterminant interfaces result in different forms of the coefficient matrices $[m_q]_i$, $[c_q]_i$, and $[k_q]_i$.

A statically determinant interface exists when the interface coordinates $\{u\}_{Bi}$ represent linear combination of rigid body displacements. Although it can be greater than six, six is the maximum number for VO. The matrices are of the form

$$\begin{bmatrix}m_{qi}^{RR} & m_{qi}^{RE}\\ m_{qi}^{ER} & m_{qi}^{EE}\end{bmatrix},\begin{bmatrix}0 & 0\\ 0 & c_{qi}^{EE}\end{bmatrix},\text{ and }\begin{bmatrix}0 & 0\\ 0 & k_{qi}^{EE}\end{bmatrix} \quad (16)$$

where superscripts

R = rigid body motion

E = elastic motion

Statically indeterminant interface coordinates $\{u\}_{Bi}$ have more interface coordinates than can be represented by a linear combination of rigid body displacements. The matrices are of the form

$$\begin{bmatrix}m_{qi}^{II} & m_{qi}^{IO}\\ m_{qi}^{OI} & m_{qi}^{OO}\end{bmatrix},\begin{bmatrix}c_{qi}^{II} & c_{qi}^{IO}\\ c_{qi}^{OI} & c_{qi}^{OO}\end{bmatrix},\text{ and }\begin{bmatrix}k_{qi}^{II} & k_{qi}^{IO}\\ k_{qi}^{OI} & k_{qi}^{OO}\end{bmatrix} \quad (17)$$

where superscripts

I = interface motion

O = other than interface motion

Equation (16) is a special form of Eq. (17).

J. Equation of Motion of Total Structure

If each substructure is considered as a finite element, they can be combined with the

bus in a way similar to Eqs. (2) and (4). The results are

$$[M]\begin{Bmatrix}\{\ddot{u}\}_R\\ \{\ddot{u}\}_B\\ \{\ddot{q}\}_1\\ \vdots\\ \{\ddot{q}\}_i\end{Bmatrix}+[C]\begin{Bmatrix}\{\dot{u}\}_R\\ \{\dot{u}\}_B\\ \{\dot{q}\}_1\\ \vdots\\ \{\dot{q}\}_i\end{Bmatrix}+[K]\begin{Bmatrix}\{u\}_R\\ \{u\}_B\\ \{q\}_1\\ \vdots\\ \{q\}_i\end{Bmatrix}=\{0\} \tag{18}$$

$$\{P\}_B = [S]\{u\}_B$$

$$\{P\}_i = [S][\phi]_i\{u\}_i$$

where

$\{u\}_R$ = rigid body degrees of freedom of the V-S/C or the motions at the V-S/C/Centaur interface

$[\phi]_i$ = displacement function of i^{th} substructure

$\{u\}_i$ = real displacements of i^{th} substructure

$\{P\}_B$ = member forces in the bus

$\{P\}_i$ = member forces in i^{th} substructure

The eigenvalues and eigenvectors of Eq. (18) with terms associated with $[C]$ and $\{u\}_R$ removed are $[\omega^2]$ and $[\phi]$. Substitution of the transformation

$$\begin{Bmatrix}\{u\}_B\\ \{q\}_1\\ \vdots\\ \{q\}_i\end{Bmatrix}=[\phi]\{X\} \tag{19}$$

into Eq. (18) and premultiplication by $[\phi]^T$ results in

$$[\overline{M}]\begin{Bmatrix}\{\ddot{u}\}_R\\ \{\ddot{X}\}\end{Bmatrix}+[\overline{C}]\begin{Bmatrix}\{\dot{u}\}_R\\ \{\dot{X}\}\end{Bmatrix}+[\overline{K}]\begin{Bmatrix}\{u\}_R\\ \{X\}\end{Bmatrix}=\{0\} \tag{20}$$

where

$$[\overline{M}]=\begin{bmatrix}\overline{M}^{RR} & \overline{M}^{RE}\\ \overline{M}^{ER} & \overline{M}^{EE}\end{bmatrix}$$

$$\left[\overline{M}^{EE}\right]=[\phi]^T[M][\phi]$$

$$[\overline{C}]=\begin{bmatrix}0 & 0\\ 0 & \left[\overline{C}^{EE}\right]\end{bmatrix} \tag{21}$$

$$\left[\overline{C}^{EE}\right]=\left[2\rho_i\sqrt{\overline{M}^{EE}\,\overline{K}^{EE}}\right]$$

where ρ_i is the critical viscous damping ratio,

$$[\overline{K}]=\begin{bmatrix}0 & 0\\ 0 & \left[\overline{K}^{EE}\right]\end{bmatrix}$$

$$\left[\overline{K}^{EE}\right]=[\phi]^T[K][\phi]=\left[\overline{M}^{EE}\,\omega^2\right]$$

The significance of the rigid VLC is illustrated. Since the VLC attachment to the VO is statically determinant, from Eq. (16)

$$\begin{bmatrix}M_{qL}^{RR} & M_{qL}^{RE}\\ M_{qL}^{ER} & M_{qL}^{EE}\end{bmatrix},\ \begin{bmatrix}0 & 0\\ 0 & C_{qL}^{EE}\end{bmatrix},\ \text{and}\ \begin{bmatrix}0 & 0\\ 0 & K_{qL}^{EE}\end{bmatrix}$$

where i = L is the symbol used for the VLC. Combination of the mass matrix of the VLC with the bus can be shown as

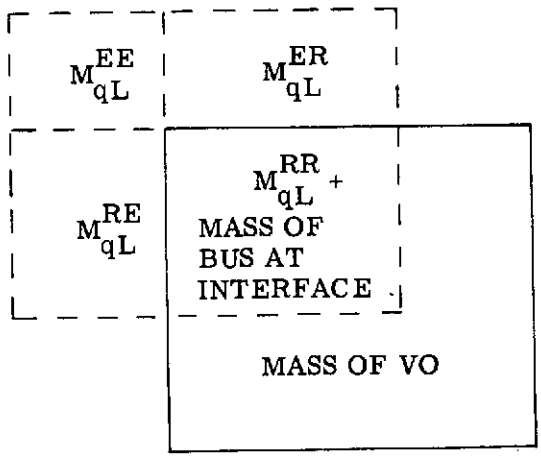

The damping and stiffness matrices do not couple. Thus the physical addition of the rigid VLC is equivalent to adding $[m_{qL}^{RR}]$ to the mass matrix of the VO. No other VLC parameters are included in the VO analysis.

The equations are derived for a system with small damping where the eigenvectors of the undamped equation can be assumed to diagonalize the original damping matrix. This is assumed for VO although discrete viscous dampers exist. See Ref. (6) for treatment of viscous dampers.

K. Size of the Problem

The approximate size of the VO dynamic model used for Load Analysis is summarized in Table 3.

SUBSTRUCTURE TESTS AND ANALYSIS CORRELATION

During the program, information on substructures, structural components, and parameters related to dynamics were obtained during the development test program. The tests were run to

(1) Directly obtain dynamic data.

(2) Establish feasibility of future tests.

The principal objectives of many tests were other than obtaining data to verify models.

Two tests to be discussed illustrate the procedure used in correlating the mathematical model with the test data.

A. Propulsion Module Modal Test

Figure 4 shows the propulsion module modal test setup. The objectives of the test were to:

(1) Establish the difficulty of performing a modal test with ullage in the tanks. (Both a zero ullage and ullage conditions were tested.)

(2) Establish nonlinearity of the system with excitation force.

(3) Establish the influence of the tank pressure on its dynamic characteristics.

(4) Measure the eigenvectors and eigenvalues.

(5) Indirectly measure the constraint modes.

(6) Measure the modal force transformations.

The changes in the model as a result of the test are shown in Tables 4, 5, and 6.

TABLE 3
Size of VO Dynamic Model

Substructure	Elastic DOF	Dynamic DOF	Interface DOF	Normal Modes
Rigid lander and bus	1,720	153	75	0
Scan platform	580	84	14	3
Solar panels	3,444	452	28	20
Cable trough	192	153	20	0
Propulsion module	695	78	16	12
3-hole tab	20,000	0	192	0
Mickey mouse tab	3,400	0	24	0
Siamese tab	1,760	0	22	0
CTA/VTA	42	0	36	0

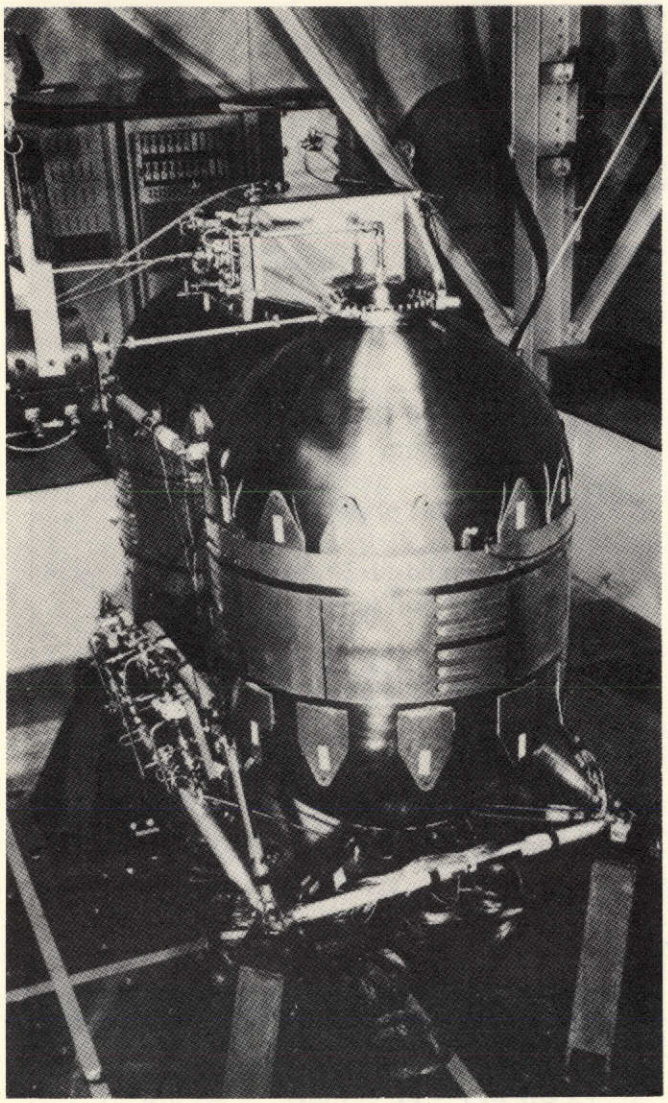

Fig. 4 - Propulsion module modal test

B. Solar Panel Modal Test

Figure 5 shows the solar panel modal test setup. A brief description of the results is shown in Table 7.

Since the mode shapes of the analysis and the test compared well, only the frequencies of the modes were changed. Extraneous modes from the analysis were eliminated. The modal test was performed on the solar panel with the relay antenna. The solar panel model result without the relay antenna was obtained analytically using the model with the relay antenna adjusted to the test data.

SYSTEM MODAL TEST AND ANALYSIS CORRELATION

A. Modal Test Configuration

As illustrated in Fig. 2, the VO system modal test configuration did not duplicate the flight configuration. The objective was to verify as many significant substructures and their interactions as feasible. The modal test configuration is represented by the equations

$$[0] = [M]_{T,A} \begin{Bmatrix} \{\ddot{u}\}_R \\ \{\ddot{u}\}_B \\ \{\ddot{q}\}_{P,T} \\ \{\ddot{q}\}_{S,T} \\ \{\ddot{q}\}_C \end{Bmatrix} + [C]_{T,A} \begin{Bmatrix} \{\dot{u}\}_R \\ \{\dot{u}\}_B \\ \{\dot{q}\}_{P,T} \\ \{\dot{q}\}_{S,T} \\ \{\dot{q}\}_C \end{Bmatrix} + [K]_{T,A} \begin{Bmatrix} \{u\}_R \\ \{u\}_B \\ \{q\}_{P,T} \\ \{q\}_{S,T} \\ \{q\}_C \end{Bmatrix} \quad (22)$$

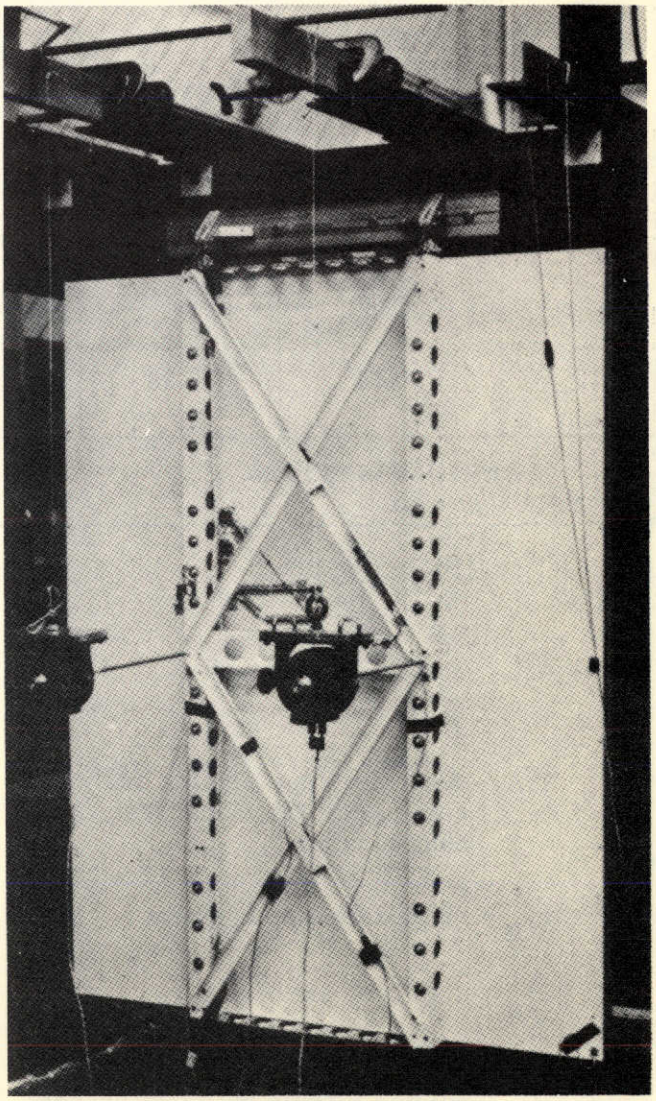

Fig. 5 - Solar panel modal test

TABLE 4
Frequency Change and Damping of Propulsion Subsystem Modal Test

Mode No.	Pretest Model (Hz)	Modal Test (Hz)	Posttest Model (Hz)	Mode Description	Damping Ratio
1	12.11	12.95	12.95	Oxidizer and fuel tanks in Y direction (in phase)	0.010
2	14.90	17.66	16.36	Oxidizer tank in Z direction	0.0049
3	19.24	20.80	19.83	Oxidizer and fuel tanks in Z direction	0.0084
	22.43			Local thrust plate	
4	25.76	22.97	26.70	Oxidizer and fuel tank in Y direction (out of phase)	
5	27.50	28.33	28.30	Fuel tank in Z direction	0.0074
	35.57			Local PCA	
6	38.67	32.76	34.25	Pressurant tank in θ_Y direction*	0.0106
7		42.80†	45.75	Local PCA in X direction†	
8	41.62	50.67	49.69	Pressurant tank in Y direction	0.0078
12	50.54	65.38	65.67	PCA in θ_Y direction	0.0107

*θ_Y is rotation in radians
†MMA test data

$$\{P\}_B = [S]\{u\}_B$$

$$\{P\}_i = [S][\phi]_i\{u\}_i$$

where

T,A = subscript representing analytical estimate of the modal test configuration

$\{u\}_R$ = rigid body displacement

$\{u\}_B$ = displacement of bus

$\{q\}_{P,T}$ = generalized coordinate of propulsion module with test propellant mass (see Table 2)

$\{q\}_{S,T}$ = generalized coordinate of the scan platform in test configuration; joints are not allowed to slip along the serration

$\{q\}_C$ = generalized coordinate of the cable trough

In steps identical to obtaining Eqs. (19) through (21), one obtains from Eq. (22):

eigenvalues,

$$\left[\omega^2\right]_{T,A} \tag{22a}$$

eigenvectors,

$$[\phi]_{T,A} \tag{22b}$$

TABLE 5
Kinetic Energy Distribution of Propulsion Module Modal Test

Mode			Pretest Analysis (%)	Modal Test (%)	Posttest Analysis (%)
12.95 Hz	Oxidizer tank	X			
		Y	63.38	76.76	68.17
		Z			
	Fuel tank	X			
		Y	21.41	18.04	24.27
		Z			
17.66 Hz	Oxidizer tank	X	33.11	23.63	34.02
		Y			
		Z	25.39	50.09	35.12
	Fuel tank	X	15.65	13.81	16.72
		Y			
		Z	2.89	0.71	2.22
20.80 Hz	Oxidizer tank	X	13.83	26.96	19.27
		Y			
		Z	58.56	38.83	49.82
	Fuel tank	X	2.33	6.22	3.52
		Y			
		Z	19.03	22.34	22.04
22.97 Hz	Oxidizer tank	X			
		Y	22.14	21.82	23.26
		Z			
	Fuel tank	X	0.84	0.02	1.22
		Y	50.75	64.18	50.08
		Z	3.27	0.09	3.66
28.33 Hz	Oxidizer tank	X	11.60	11.72	11.29
		Y	1.65	0.37	2.04
		Z	5.22	3.54	5.75
	Fuel tank	X	6.78	8.35	6.39
		Y	2.74	0.83	3.42
		Z	57.10	58.92	56.58

TABLE 6
Modal Forces of Propulsion Subsystem Modal Test

Member No.		Mode 1 (lb)	Mode 2 (lb)	Mode 3 (lb)	Mode 4 (lb)	Mode 5 (lb)
4	Pretest	-627.5	133.9	-220.4	-12.99	-43.4
	Test	-568.2	77.1	-266.1	-53.3	-43.7
	Posttest	-572.9	112.9	-237.3	-110.5	-41.9
3	Pretest	-70.8	-130.3	63.2	135.7	95.4
	Test	-66.8	-87.1	85.3	90.5	73.7
	Posttest	-73.8	-109.7	72.7	124.1	97.5
41	Pretest	469.7	-241.9	-179.2	231.6	-32.0
	Test	476.6	-252.5	-109.6	188.0	-57.4
	Posttest	427.2	-244.3	-147.8	183.4	-30.9
40	Pretest	237.6	158.6	110.2	44.7	-89.6
	Test	205.9	144.7	82.1	56.5	-53.0
	Posttest	249.2	143.7	95.6	40.4	-98.5
12	Pretest	596.2	124.0	-286.5	62.6	-64.4
	Test	497.7	82.6	-294.7	43.1	-53.3
	Posttest	549.1	95.8	-290.9	62.9	-71.2
11	Pretest	144.7	-125.9	48.6	-46.5	124.0
	Test	151.4	-99.4	79.9	-98.4	99.1
	Posttest	152.6	-108.3	58.1	-38.2	131.8
36	Pretest	-530.9	-220.4	-152.2	170.6	-60.5
	Test	-452.6	-266.1	-91.7	172.4	-61.3
	Posttest	-489.0	-220.8	-126.0	134.6	-63.9
37	Pretest	-124.0	171.5	118.9	110.5	-58.2
	Test	-197.7	120.8	89.0	-67.8	-47.8
	Posttest	-130.7	157.1	101.3	-105.3	-60.9
18	Pretest	273.8	-25.9	-127.3	-52.4	-21.1
	Test	264.9	-33.0	-121.5	-39.5	-27.7
	Posttest	309.1	-30.7	-126.5	-48.9	-17.7
8	Pretest	-299.0	-17.9	-104.4	43.5	-22.2
	Test	-292.1	38.6	-115.3	25.7	-23.9
	Posttest	-302.4	23.4	-100.0	70.5	-23.9

TABLE 7
Frequency Change and Damping of Solar Panel Modal Test

Mode No.	Pretest Math Model (Hz)	Modal Test (Hz)	Adjusted Posttest Math Model (Hz)	Damping Ratio
1	37.0	22.4	22.4	0.023
2	31.56	26.8	26.8	0.017
3	34.55	31.0	31.0	0.030
4	40.11	–	–	–
5	45.17	38.5	38.5	0.030
6	59.70	57.5	59.70	0.030
7	62.32	64.9	–	–

transformation,

$$\begin{Bmatrix} \{\ddot{u}\}_B \\ \{\ddot{q}\}_{P,T} \\ \{\ddot{q}\}_{S,T} \\ \{\ddot{q}\}_C \end{Bmatrix} = [\phi]_{T,A} \{X\}_{T,A} \tag{22c}$$

equation of motion,

$$[\bar{M}]_{T,A} \begin{Bmatrix} \{\ddot{u}\}_R \\ \{\ddot{X}\}_{T,A} \end{Bmatrix} + [\bar{C}]_{T,A} \begin{Bmatrix} \{\dot{u}\}_R \\ \{\dot{X}\}_{T,A} \end{Bmatrix}$$

$$+ [\bar{K}]_{T,A} \begin{Bmatrix} \{u\}_R \\ \{X\}_{T,A} \end{Bmatrix} = \{0\} \tag{22d}$$

and force transformations,

$$\{P\}_B = [S][\phi]_{T,A} \{X\}_{T,A} \tag{22e}$$

$$\{P\}_i = [S][\phi]_i [\phi]_{T,A} \{X\}_{T,A} \tag{22f}$$

The above values are the analytical predictions of the modal test configuration.

The $[\bar{M}]_{T,A}$ term of Eq. (22d) can be expressed similarly to Eq. (21) as

$$[\bar{M}]_{T,A} = \begin{bmatrix} \bar{M}^{RR}_{T,A} & \bar{M}^{RE}_{T,A} \\ \bar{M}^{ER}_{T,A} & \left[\bar{M}^{EE}_{T,A}\right] \end{bmatrix} \tag{22g}$$

$$\left[\bar{M}^{EE}_{T,A}\right] = [\phi]^T_{T,A} [M]_{T,A} [\phi]_{T,A} \tag{22h}$$

B. Correlation

The objective of the correlation of modal test data and analysis is to verify the mathematical model as shown in Eq. (22). However, this mathematical model is in a hybrid system, i.e., some degrees of freedom are expressed in the physical coordinates and others are in the generalized coordinates. The hybrid system is a result of the modal coupling technique used in the analysis. For a direct comparison, the solutions of Eq. (22) must be expressed in the form compatible to the measured test results. For this purpose, the normal modes obtained from Eq. (22) are transformed into the accelerometer locations.

$$[\phi']_{T,A} = [T][\phi]_{T,A} \tag{23}$$

where

$[\phi']_{T,A}$ = analytical mode expressed at accelerometer locations

$[\phi]_{T,A}$ = normal mode solution of Eq. (22)

$[T]$ = transformation matrix

In Eq. (22), 1773 degrees of freedom exist in the hybrid coordinates, whereas $[\phi']_{T,A}$ involves only 153 degrees of freedom. Because the accelerometer locations often do not coincide with the analytical node points, Eq. (23) is an approximation.

For the modal test, a test mass matrix $[M]_T$ was constructed based upon physical mass distribution and corresponded to the experimental accelerometer measurements. Throughout the correlation, the analytical predictions reduced to the accelerometer degrees of freedom [Eq. (23)] and the $[M]_T$ are used. The use of the $[M]_{T,A}$ of Eq. (22) is complicated because it contains masses corresponding to hybrid coordinates and the degrees of freedom of the test modes must be matched to correspond to the analytical degrees of freedom. The validity of $[M]_T$ is verified with the solution of Eq. (22) by the mixed orthogonality check.

$$[\phi]^T_{T,A}[M]_T[\phi']_{T,A} = [\bar{M}']_{T,A} \quad (24)$$

Ideally $[\bar{M}']_{T,A}$ is a diagonal matrix, however, as shown in Table 8, there are off-diagonal terms. In general for the first twelve modes, the off-diagonal terms are very small (less than 5%). This indicates that $[M]_T$ is indeed a valid mass matrix representing the total structural system for the first 12 modes. Additionally the magnitude of the off-diagonal terms indicates the best accuracy one can expect in an orthogonality check of the test modes with the $[M]_T$. Since a more detailed mass distribution was used in the analysis than in the modal test data reduction program, the orthogonality of $[\bar{M}']_{T,A}$ deteriorates for the higher frequency modes.

The test modal data together with analytical prediction $[\phi']_{T,A}$ and $[M]_T$ are read into the computer file for processing. The correlation work is automated.

C. Mode Identification

Prior to any correlation, the identification of test modes to the corresponding analytical modes is required. This task is achieved by the following criteria:

$$\{\bar{M}\}_T = [\phi']_{T,A}[M]_T\{\phi_j\}_T \quad (25)$$

Here the j^{th} test mode is checked with all the analytical modes $[\phi']_{T,A}$. The j^{th} test mode corresponds to the analytical mode related to the largest k^{th} term in $\{M\}_T$. A perfect correlation exists when the k^{th} term is unity with all the other terms zero. After the identification of a test mode to an analytical mode, the correlation program calculates the necessary information required for a detailed comparison between the test and analysis. Table 9 shows the cross-orthogonality check between the test mode 701 and the first 30 analytical modes. For this case, the test mode 701 corresponds to the third analytical mode.

TABLE 8
Mixed Orthogonality – Model VIII

4.35	4.40	7.48	7.83	10.92	13.36	14.64	17.95	18.81	23.42	24.28	26.18 ← Frequency (Hz)	
1	2	3	4	5	6	7	8	9	10	11	12 ← Mode	
100	0.9	-0.3	-0.2	0.8	-0.9	1.4	1.6	-1.7	-0.3	-0.9	0.4	1
	100	-0.2	-0.2	0.3	0.1	-0.1	0.2	-3.1	0.4	-2.2	-0.4	2
		100	1.3	-1.6	1.1	-1.7	-1.4	0	-2.1	-1.2	0.7	3
			100	-0.4	1.2	-0.2	-0.3	-2.7	1.7	-.03	1.1	4
				100	1.0	0.8	1.1	-0.6	2.2	-0.2	1.1	5
					100	0.4	-0.7	0.8	0.9	-0.9	1.8	6
						100	-1.8	0	0.2	-2.3	0.9	7
							100	-0.2	-1.4	1.2	-0.2	8
								100	-0.9	0.7	-1.4	9
									100	-1.0	0.2	10
										100	-2.3	11
											100	12

TABLE 9
Cross Orthogonality – Orthogonality of Test Mode No. 701; Run Name DTA701 at Frequency 7.84 Hz with Respect to All Analytical Modes

Analytical-Mode No.	Freq	Ortho
1	4.35	-.001
2	4.40	-.005
3	7.48	-.997
4	7.83	-.015
5	10.92	-.003
6	13.36	-.015
7	14.64	.006
8	17.95	.023
9	18.81	.000
10	23.42	.006
11	24.28	.011
12	26.18	-.008
13	28.72	.001
14	29.98	.001
15	31.36	-.020
16	33.54	-.009
17	34.68	.004
18	35.80	-.000
19	36.95	.011
20	38.43	.002
21	39.11	-.088
22	40.58	-.051
23	42.05	-.015
24	43.15	-.003
25	45.32	-.004
26	45.80	-.011
27	51.80	.003
28	52.40	-.007
29	53.15	.008
30	59.44	-.010
CORRELATION CHOICE 1 ANALYTICAL MODE 3		FREQUENCY 7.48

D. Modal Test Equation

The mathematical equation governing the modal test structural system is:

$$\{f\}_T e^{i\omega t} = [M]_T \{\ddot{u}\}_T + [C]_T \{\dot{u}\}_T + [K]_T \{u\}_T \quad (26)$$

where

$\{u\}_T$ = displacement vector for each DOF associated with accelerometer measurement

$[M]_T$ = test mass matrix

$[C]_T$ = test damping matrix

$[K]_T$ = stiffness matrix

$\{f\}_T$ = force vector from the shaker

In contrast to the modal analysis as shown by the homogeneous Eq. (22), Eq. (26) is a forced response equation. The external harmonic excitation is provided by the shakers used in the modal test. The solution of Eq. (26) can be expressed in terms of generalized coordinates as follows:

$$\{u\}_T = [\phi]_T \{q\}_T \quad (27)$$

where $[\phi]_T$ is the normal mode matrix, which is the eigenvectors of the test configuration measured at accelerometer locations. Substitution of Eq. (27) into Eq. (26) and premultiplication by $[\phi]_T^T$ result in

$$[\phi]_T^T \{f\}_T e^{i\omega t} = [\overline{M}]_T \{\ddot{q}\}_T + [\overline{C}]_T \{\dot{q}\}_T + [\overline{K}]_T \{q\}_T \quad (28)$$

where

$$[\overline{M}]_T = [\phi]_T^T [M]_T [\phi]_T$$

generalized mass (28a)

$$[\overline{K}]_T = [\phi]_T^T [K]_T [\phi]_T$$

generalized stiffness (28b)

$$[\overline{C}]_T = [\phi]_T^T [C]_T [\phi]_T$$

generalized damping (28c)

$$\omega_n = \sqrt{\overline{K}_n / \overline{M}_n}$$

n^{th} eigenvalue (28d)

The accelerometer measurements obtained during the test are the response from the shaker force instead of the normal modes. The response is expressed as:

$$\{u\}_T = [\phi]_T [H_n(\omega)] [\phi]_T^T \{f\}_T e^{i\omega t} \quad (29)$$

where

$$H_n(\omega) = \frac{\omega_n^2/\bar{K}_n}{\left(\omega_n^2 - \omega^2\right) + i\,2\,\rho_n\omega\;\omega_n}$$

When the shaker frequency ω is tuned to one of the natural frequencies ω_n, only one term in the $[H_n(\omega)]$ dominates if ρ_n, the percentage of critical damping, is very small and all the natural frequencies are well separated. Thus the following approximation may be obtained:

$$\{u\}_T \cong \{\phi_T\}_n$$

A relatively "clean" normal mode can be measured when damping is small and the natural frequencies of the structure are well separated. In general, the damping of the structure is indeed very small but not all the natural frequencies are well separated. Hence, errors are expected when two normal mode frequencies are not well separated.

E. Modal Test Output

The output of the modal test is

eigenvector,

$$[\phi]_T \tag{30a}$$

eigenvalue,

$$[\omega^2]_T \tag{30b}$$

and modal force coefficients

$$\{P\}_T \tag{30c}$$

Evaluating the generalized mass matrix similarly to Eq. (22g), including the masses corresponding to the rigid body displacements, results in

$$[\bar{M}]_T = \begin{bmatrix} \bar{M}_T^{RR} & \bar{M}_T^{RE} \\ \bar{M}_T^{ER} & [\bar{M}_T^{EE}] \end{bmatrix} \tag{30d}$$

where

$$[\bar{M}_T^{EE}] = [\bar{M}]_T \tag{30e}$$

of Eq. (28a). Equations (30a) through (30e) are compared to Eqs. (22a), (22b), and (22e) through (22h).

F. Frequency

The first data correlated are the natural frequencies. Table 10 lists the natural frequencies from analysis and corresponding test frequencies together with the mode description for the first twelve modes. Except for the eleventh mode, which is a scan platform mode, all the frequencies match fairly well.

G. Orthogonality

The generalized mass, Eq. (28a), is normalized to a unit matrix by proper normalization of each individual mode. Ideally,

$$[\bar{M}]_T = [\phi]_T^T [M]_T [\phi]_T = [I] \tag{31}$$

Any errors in the mode shape measurement or mass data produce finite off-diagonal terms in the generalized mass matrix. If all off-diagonal terms are small, the measured normal modes are orthogonal to each other with respect to the mass matrix. Therefore, the orthogonality check serves as an indication of the accuracy of the measured test modes and test mass matrix. The orthogonality check of the first twelve test modes is in Table 11. The off-diagonal terms are indeed small and are within the 10% goal established for the test. The largest term occurs between the first and second modes. Since Table 10 indicates the natural frequencies of the first two modes to be almost identical, accurate mode shape measurements for these two modes are difficult to obtain.

H. Effective Mass (Ref. 7)

In principle, the number of independent normal modes in a structural system is equal to the number of degrees of freedom. Obviously some of these modes are highly localized and of minor importance as far as the load analysis is concerned. With a limited number of modes obtained in the modal test, criteria are required to establish that the measured modes include the significant structural modes. For this purpose, the generalized rigid-body mass is used in the following way. In the analysis, the generalized rigid-body mass is defined, as in Eq. (22g), as $[\bar{M}^{RR}]_{T,A}$ or

$$\left[\bar{M}^{RR}\right]_{T,A} = \left[\{u\}_R\right]^T [M]_{T,A} \left[\{u\}_R\right] \tag{32a}$$

TABLE 10
Modal Frequency Comparison

Mode	Frequency (Hz)			Description
	Analysis	Test	Error (%)	
1	4.35	4.51	3.5	Bending in X
2	4.40	4.63	5.0	Bending in Y
3	7.48	7.87	5.0	Lander in θ_Z
4	7.83	8.30	5.7	Lander in Y
5	10.92	11.51	5.1	Lander in X
6	13.36	14.09	5.2	Lander in θ_Y
7	14.64	15.35	4.6	Oxidizer tank in Z
8	17.95	19.49	7.9	Fuel tank in Z
9	18.81	19.83	5.1	Lander in θ_X
10	23.42	24.85	5.8	Fuel tank in Y
11	26.18	29.54	11.4	Scan platform in θ_Y
12	24.28	26.49	8.3	Lander in Z

TABLE 11
Orthogonality

Mode ↓ \ →	1	2	3	4	5	6	7	8	9	10	11	12
1	100.0	6.2	-0.2	1.1	-0.3	1.1	-2.3	-0.6	-1.7	0.6	-2.4	0.0
2		100.0	0.1	-1.2	-4.1	-3.0	-0.9	-2.5	1.0	1.2	3.4	-1.5
3			100.0	0.4	0.8	1.6	-0.2	3.5	-1.5	-0.5	-0.7	0.4
4				100.0	1.0	1.3	1.2	-0.1	-1.8	1.2	1.1	-0.5
5					100.0	0.6	0.8	4.6	-1.0	0.2	1.7	-0.4
6						100.0	0.4	-0.5	1.3	4.4	-0.6	1.6
7							100.0	-0.2	-0.1	3.6	-0.1	-1.3
8								100.0	-1.1	-1.9	-0.2	-1.5
9									100.0	5.9	-2.9	2.7
10										100.0	1.0	-3.4
11											100.0	2.5
12												100.0

From the modal test results of Eq. (30d),

$$\left[\bar{M}^{RR}\right]_T = \left[\{u\}_R\right]^T \left[M\right]_T \left[\{u\}_R\right] \quad (32b)$$

An experimental generalized rigid-body-mass derived from $\left[\bar{M}^{RE}\right]_T$ is defined as

$$\left[\bar{\bar{M}}^{RR}\right]_T = \left[\bar{M}^{RE}\right]_T \left[I\right] \left[\bar{M}^{ER}\right]_T \quad (33)$$

where

$$\left[\bar{M}^{RE}\right]_T = \left[\{u\}_R\right]^T \left[M\right]_T \left[\Phi\right]_T \quad (34)$$

$$\left[\bar{M}^{ER}\right]_T = \left[\bar{M}^{RE}\right]_T^T \quad (35)$$

If all the experimental modes are obtained, it can be proved that

$$\left[\bar{\bar{M}}^{RR}\right]_T = \left[\bar{M}^{RR}\right]_T \cong \left[\bar{M}^{RR}\right]_{T,A} \quad (36)$$

Another check is $\left[\bar{M}^{RR}\right]_T$ must be equal to the rigid body inertia property of the test configuration.

In the modal test, a limited number of measured modes was used to calculate the $\left[\bar{\bar{M}}^{RR}\right]_T$, now defined as effective mass. The comparison of $\left[\bar{\bar{M}}^{RR}\right]_T$ and $\left[\bar{M}^{RR}\right]_T$ indicates whether the major modes were effectively surveyed. If $\left[\bar{\bar{M}}^{RR}\right]_T$ is close to $\left[\bar{M}^{RR}\right]_T$, the major important modes with respect to the restrained point were obtained. Table 12 shows the summary of the effective mass of the first twelve test modes and corresponding analytical modes. The first twelve modes represent over 90% of the effective mass with respect to the base of the VTA/CTA.

TABLE 12
Effective Mass in Percentage

Mode		Mass					
		X (%)	Y (%)	Z (%)	θ_x (%)	θ_y (%)	θ_z (%)
1	Analysis	96.42	1.76	0.01	1.34	85.20	0.14
	Test	89.51	7.97	0.03	6.12	78.23	0.88
2	Analysis	1.67	87.47	0.0	63.66	1.49	1.09
	Test	3.30	86.49	0.03	64.45	3.15	1.13
3	Analysis	0.95	0.28	0.0	1.75	0.02	55.21
	Test	0.89	0.35	0.01	1.88	0.02	56.91
4	Analysis	0.06	5.60	0.03	28.95	0.01	1.94
	Test	0.10	4.81	0.10	27.51	0.0	1.66
5	Analysis	0.05	0.06	0.56	0.10	6.40	19.58
	Test	0.0	0.11	0.58	0.19	7.80	20.43
6	Analysis	0.20	0.06	5.63	0.10	4.77	9.83
	Test	0.38	0.01	6.67	0.01	5.65	7.39
7	Analysis	0.0	0.01	49.02	0.01	0.40	0.25
	Test	0.01	0.0	51.80	0.0	0.63	0.24
8	Analysis	0.02	0.01	12.98	0.01	0.04	0.07
	Test	0.02	0.0	12.52	0.01	0.0	0.15
9	Analysis	0.0	0.06	0.45	0.06	0.0	0.41
	Test	0.0	0.05	0.90	0.02	0.0	0.09

TABLE 12
Effective Mass in Percentage (contd)

Mode		Mass					
		X (%)	Y (%)	Z (%)	θ_x (%)	θ_y (%)	θ_z (%)
10	Analysis	0.0	0.02	3.15	0.03	0.0	0.0
	Test	0.0	0.01	0.58	0.03	0.01	0.04
11	Analysis	0.0	0.02	13.60	0.07	0.0	0.23
	Test	0.0	0.01	11.57	0.02	0.0	0.06
12	Analysis	0.0	0.02	5.02	0.06	0.0	0.0
	Test	0.0	0.07	22.17	0.20	0.0	0.06
Total	Analysis	99.37	95.37	90.45	96.12	98.33	88.75
	Test	94.39	100.24	95.96	100.20	95.89	89.15

I. Mode Shape

The eigenvectors or mode shapes are important in the load analysis. The mode shape is expressed in the form of modal deflections of each degree of freedom (DOF). In the mathematical model, each DOF is assigned to a number shown in Fig. 2, the ODTM modal test configuration. The direction of the modal deflection is indicated by the last digit in the DOF. Translation in X, Y, and Z are 1, 2, and 3 respectively. For example, 1013 represents the motion of node 101 in the Z direction. The modal deflection of each DOF is expressed in their own local coordinate system, which is shown in Figs. 6 to 10.

The maximum amplitudes of the modal deflection are normalized to unity. The analysis and test are compared and the difference at each DOF is expressed as a weighted deviation (WD) defined as

$$WD = \left[[\phi']_{T,A} - [\phi]_T \right] \text{ normalized} \tag{37a}$$

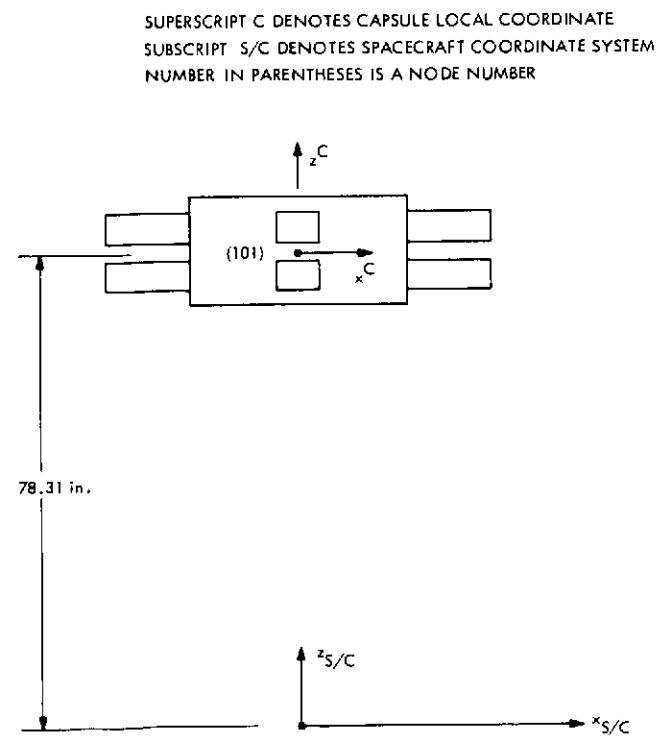

Fig. 6 - Local coordinate of VLC

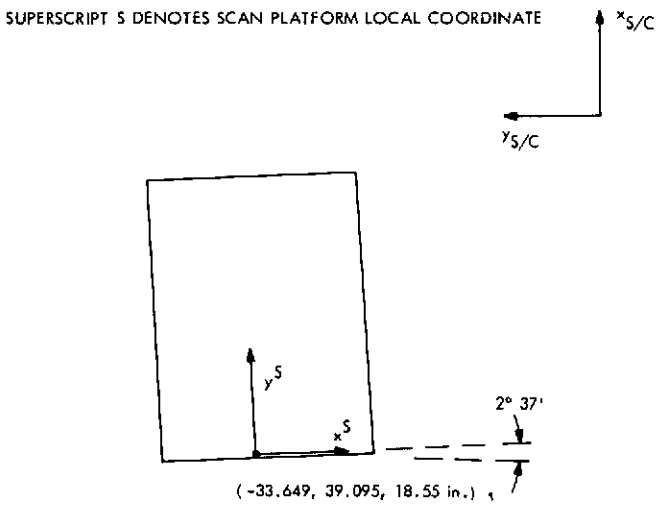

Fig. 7 - Local coordinate of scan platform

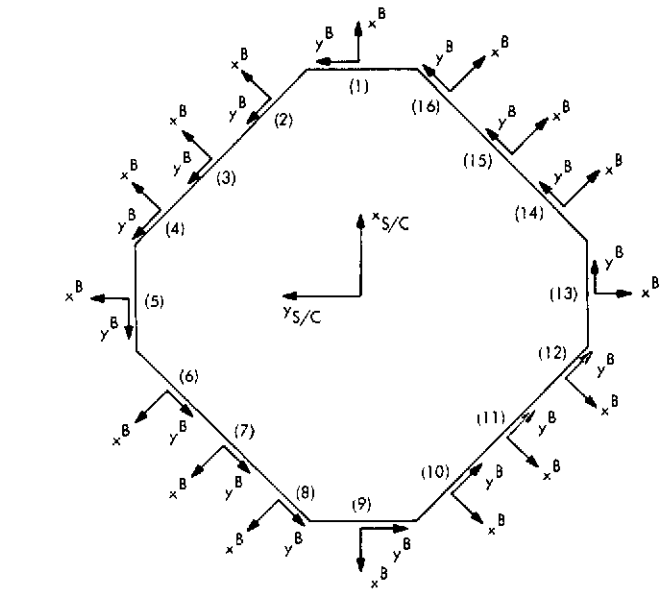

Fig. 8 - Local coordinate of bus

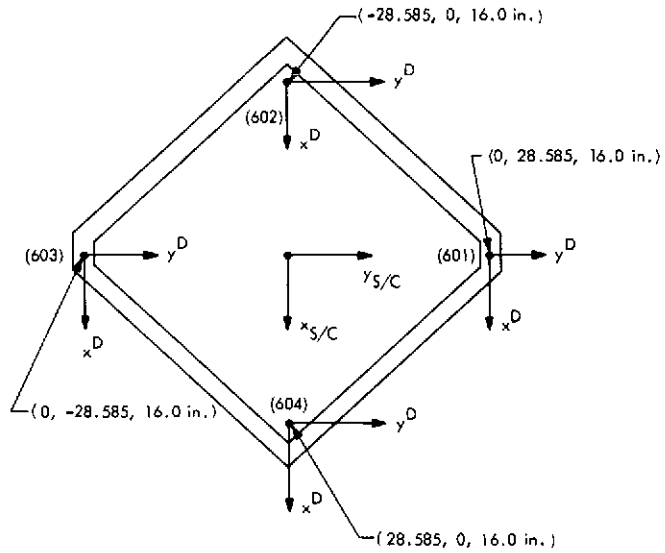

Fig. 9 - Local coordinate of cable trough

Also, for each mode the standard deviation (RSS) is calculated as

$$\mathrm{RSS} = \left[\frac{1}{N}\sum_{i=1}^{N}(\mathrm{WD})_i^2\right]^{1/2} \qquad (37b)$$

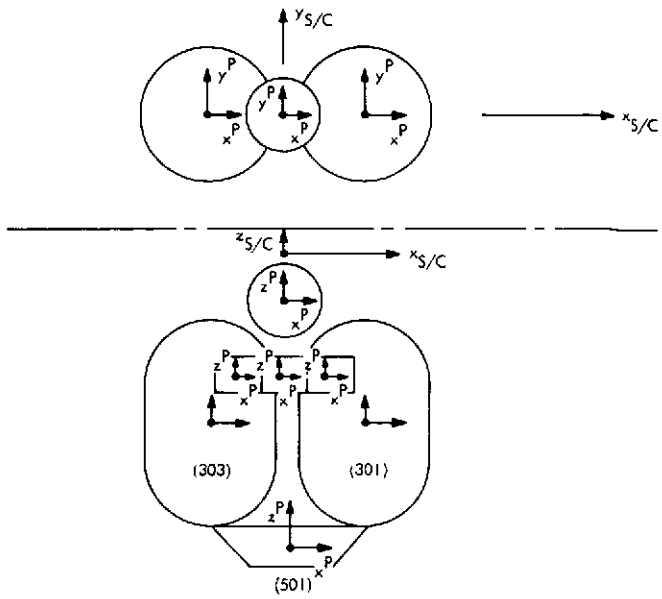

Fig. 10 - Local coordinate of propulsion module

where

N = number of DOF

$(\mathrm{WD})_i$ = weighted deviation of i^{th} DOF

In Tables 13 and 14, a typical mode shape comparison of a mode and the summary comparison of the first few modes, with only the important DOF and the standard deviations, are given.

TABLE 13
Modal Comparison – Analytical Mode 3 vs Experimental Mode 701

DOF	Analysis	Test	Weighted Deviation
11	.346+00	.370+00	-.247-01
12	.666+00	.655+00	.109-01
13	.784-01	.490-01	.295-01
14	-.418-02	-.319-02	-.994-03
15	-.417-02	-.225-02	-.192-02
16	.101-01	.119-01	-.181-02
21	.505+00	.542+00	-.369-01
22	.284+00	.279+00	.568-02
23	.314-01	.459-01	-.145-01
24	-.260-02	.213-03	-.282-02
25	-.389-02	.254-02	-.643-02
26	.608-02	.958-02	-.351-02
31	.268+00	.286+00	-.178-01
32	.272+00	.226+00	.452-01
33	.747-01	.636-01	.111-01

TABLE 13
Modal Comparison – Analytical Mode 3 vs Experimental Mode 701 (contd)

DOF	Analysis	Test	Weighted Deviation
34	-.314-02	-.112-02	-.202-02
35	.968-02	.570-02	.399-02
36	.707-02	.162-01	-.913-02
41	-.914-02	-.189-01	.972-02
42	.314+00	.299+00	.147-01
43	.696-01	.755-01	-.593-02
44	-.895-03	.263-02	-.353-02
45	-.115-01	-.171-02	-.981-02
46	.748-02	.129-01	-.538-02
51	-.106+00	-.110+00	.312-02
52	.353+00	.325+00	.281-01
53	.140+00	.121+00	.187-01
54	-.923-03	.282-02	-.375-02
55	-.143-01	-.889-02	-.544-02
56	.820-02	.133-01	-.506-02
61	-.847-01	-.966-01	.119-01
62	.403+00	.322+00	.804-01
63	.135+00	.113+00	.229-01
64	-.854-02	-.347-02	-.507-02
65	-.976-02	-.824-02	-.152-02
66	.139-01	.158-01	-.188-02
71	-.309+00	-.397+00	.878-01
72	.474+00	.507+00	-.328-01
73	.707-01	.137+00	-.665-01
74	-.364-02	-.447-02	.827-03
75	.496-02	-.124-01	.173-01
76	.145-02	.146-01	-.132-01
81	-.561+00	-.551+00	-.980-02
82	.399+00	.366+00	.327-01
83	.346-01	-.388-01	.734-01
84	-.982-02	-.216-02	-.766-02
85	-.119-01	-.917-02	-.270-02
86	.115-01	.155-01	-.396-02
91	-.297+00	-.291+00	-.617-02
92	.806+00	.816+00	-.967-02
93	-.756-01	-.999-01	.243-01
94	-.976-02	-.669-02	-.307-02
95	-.121-02	-.782-02	.662-02
96	.100-01	.520-02	.482-02
101	.186+00	.167+00	.195-01
102	.851+00	.931+00	-.800-01
103	-.161+00	-.819-01	-.786-01
104	.816-03	-.629-02	.711-02
105	-.856-03	.230-02	-.315-02
106	-.208-02	-.172-02	-.351-03
111	-.949-01	-.106+00	.108-01
112	.864+00	.824+00	.409-01
113	-.124+00	-.312-02	-.121+00
114	-.108-01	-.352-03	-.104-01
115	.195-01	.227-01	-.326-02
116	.103-01	.913-02	.118-02
121	-.409+00	-.361+00	-.488-01
122	.953+00	.100+01	-.468-01
123	-.187+00	-.985-01	-.889-01
124	-.166-02	.239-02	-.405-02
125	-.475-02	.382-01	-.429-01
126	.401-02	.452-01	-.412-01
131	.287-01	.327-01	-.397-02

TABLE 13
Modal Comparison – Analytical Mode 3 vs Experimental Mode 701 (contd)

DOF	Analysis	Test	Weighted Deviation
132	.100+01	.951+00	.491-01
133	-.140+00	-.111+00	-.287-01
134	.323-02	.513-02	-.191-02
135	-.120-01	.656-02	-.185-01
136	.915-02	.225-01	-.133-01
141	.460+00	.459+00	.825-03
142	.790+00	.691+00	.994-01
143	-.268-01	-.246-01	-.215-02
144	-.263-03	.662-02	-.688-02
145	-.106-01	-.128-02	-.935-02
146	.138-01	.195-01	-.570-02
151	.197+00	.210+00	-.129-01
152	.795+00	.744+00	.504-01
153	.500-01	-.142-01	.643-01
154	.308-02	-.193-03	.327-02
155	.141-03	-.911-02	.926-02
156	.589-02	.158-01	-.994-02
161	-.101-01	.228-01	-.329-01
162	.784+00	.770+00	.142-01
163	.690-01	.215-01	.476-01
164	-.731-03	.296-02	-.369-02
165	-.757-02	-.831-02	.738-03
166	.152-01	.111-01	.408-02
1011	-.464+00	-.460+00	-.392-02
1012	-.374+00	-.394+00	.202-01
1013	-.151-01	-.206-01	.547-02
1014	.426-02	.429-02	-.389-04
1015	.170-01	.165-01	.462-03
1016	.398-01	.426-01	-.279-02
3011	.470+00	.467+00	.239-02
3012	.419+00	.433+00	-.146-01
3013	.340-01	.175-01	.165-01
3014	.499-02	.512-02	-.126-03
3015	-.289-02	-.343-02	.541-03
3016	.164-01	.171-01	-.742-03
3031	.458+00	.452+00	.608-02
3032	-.165+00	-.196+00	.313-01
3033	-.191-01	-.426-01	.236-01
3034	.428-02	.331-02	.969-03
3035	-.267-02	-.364-02	.978-03
3036	.160-01	.168-01	-.798-03
4011	.387+00	.375+00	.121-01
4012	-.704-01	-.598-01	-.106-01
4013	.756-02	-.286-01	.362-01
4014	.373-02	.689-02	-.317-02
4015	.289-02	-.499-03	.339-02
4016	.181-01	.192-01	-.112-02
5011	.551+00	.566+00	-.148-01
5012	.244+00	.269+00	-.245-01
5013	.115-01	-.225-01	.340-01
5014	.340-02	.274-02	.652-03
5015	-.223-02	-.713-03	-.151-02
5016	.173-01	.204-01	-.313-02
2011	.687+00	.616+00	.701-01
2012	-.186+00	-.207+00	.217-01
2013	.204+00	.102+00	.102+00
2014	-.425-02	.293-02	-.718-02
2015	.106-01	.231-01	-.126-01

TABLE 13
Modal Comparison – Analytical Mode 3 vs Experimental Mode 701 (contd)

DOF	Analysis	Test	Weighted Deviation
2016	.147-01	.198-01	-.516-02
4021	.673+00	.743+00	-.698-01
4022	.120+00	.159+00	-.390-01
4023	-.756-01	-.324-01	-.432-01
4031	.673+00	.818+00	-.144+00
4032	.477-01	.833-01	-.356-01
4033	-.848-01	-.122+00	.371-01
4041	.673+00	.734+00	-.603-01
4042	-.338-01	-.465-01	.127-01
4043	-.756-01	-.120+00	.449-01
6011	-.338+00	-.266+00	-.717-01
6012	-.268+00	-.259+00	-.934-02
6013	-.600-02	.341-01	-.401-01

TABLE 13
Modal Comparison – Analytical Mode 3 vs Experimental Mode 701 (contd)

DOF	Analysis	Test	Weighted Deviation
6021	.379+00	.398+00	-.193-01
6022	-.848+00	-.852+00	.437-02
6023	.600-01	-.395-01	.996-01
6031	-.190+00	-.135+00	-.551-01
6032	.120+00	.120-01	.108+00
6033	.301-01	-.596-01	.897-01
6041	.239+00	.267+00	-.280-01
6042	.673+00	.649+00	.243-01
6043	-.379-01	.125-01	-.503-01

MAX EXPERIMENTAL AT 68
MAX ANALYTICAL AT 74
RSS ERROR= .153+00

TABLE 14
Summary of Mode Shape Comparison

Hardware	Mode 1		Mode 2		Mode 3		Mode 4		Mode 5		Mode 6		Direction
	Analysis	Test	Analysis	Test	Analysis	Test	Analysis	Test	Analysis	Test	Analysis	Test	
Lander	1.00	1.00	-0.09	0.14	0.46	0.46	-0.11	0.10	-0.81	-0.80	0.15	0.19	X
	0.10	-0.23	0.45	0.50	0.37	0.39	-1.00	-1.00	-0.04	-0.07	-0.02	-0.08	Y
		-0.01	0.01	0.02	0.02	0.02	-0.06	-0.07	0.01	0.01	-0.06	-0.07	Z
Scan platform	-0.06	0.23	-0.52	-0.48	-0.69	-0.62	0.09	0.08	-0.51	-0.45	-0.30	-0.35	X
	0.83	0.85	-0.08	0.12	0.19	0.21	-0.01	-0.02	0.85	0.75	0.92	0.94	Y
	-0.01	-0.12	0.10	0.18	-0.20	-0.10	0.29	0.30	-0.12	-0.07	0.31	0.40	Z
Bus	0.83	0.88	-0.08	0.16	-0.35	-0.37	-0.10	-0.10	0.20	0.20	0.13	0.14	X
	0.11	-0.34	0.56	0.63	-0.67	-0.66	-0.17	-0.15	-0.72	-0.63	-0.59	-0.63	Y
	0.01	0.02	0.0	0.0	-0.08	-0.05	-0.05	-0.02	0.37	0.31	-0.29	-0.31	Z
Oxid tank	0.92	0.94	-0.07	0.12	-0.47	-0.47	-0.10	-0.10	0.67	0.61	-0.17	-0.18	X
	0.17	-0.35	0.78	0.84	-0.42	-0.43	0.48	0.50	-0.24	-0.27	-0.28	-0.33	Y
	0.04	-0.02	0.0	0.01	-0.03	-0.02	0.01	0.0	0.25	0.25	-0.42	-0.52	Z
Fuel tank	0.91	0.94	-0.09	0.09	-0.46	-0.45	-0.09	-0.10	0.61	0.60	-0.16	-0.18	X
	0.16	-0.32	0.78	0.79	0.17	0.20	0.48	0.50	0.38	0.41	0.39	0.49	Y
	-0.04	-0.04	0.01	0.0	0.02	0.04	0.02	0.02	-0.15	-0.16	0.04	0.05	Z
Press tank	0.79	0.86	-0.08	0.07	-0.39	-0.38	-0.08	-0.07	0.22	0.12	0.38	0.47	X
	0.11	-0.27	0.51	0.55	0.07	0.06	-0.05	-0.05	0.06	0.07	0.85	0.79	Y
	0.0	-0.04	0.0	0.01	-0.01	0.03	0.02	0.02	0.04	0.05	-0.20	-0.26	Z
RSS	0.325		0.240		0.15		0.13		0.18		0.15		

J. Local Kinetic Energy

The generalized mass as shown in Eqs. (22h) and (28a) is expressed in the tensorial form as

$$\bar{M}_{ij}^{EE} = \sum_{\ell=1}^{N} \sum_{k=1}^{N} \Phi_{ik} M_{k\ell} \Phi_{\ell j} \qquad (38)$$

If the normal modes Φ_{ij} are in the form of velocity, $\bar{M}_{ij}^{EE}$ is in the form of kinetic energy (see Eq. (5)). Then each term in Eq. (38) represents the modal kinetic energy associated with that particular DOF. In essence, this is an itemized generalized mass. The comparison of each individual term in Eq. (38) between the test and analysis provides detailed information about the mass associated with each DOF and the modal amplitude of that DOF. This is especially valuable for those degrees of freedom where the mass is questionable, such as the propellant tanks. The standard deviation (RSS) for the local kinetic energy comparison for each mode is calculated similarly to the mode shape comparison. In Table 15, a typical mode is selected for the kinetic energy comparison. Also, in Table 16, a summary comparison of the first few modes and the standard deviation of the kinetic energy comparison is given.

TABLE 15
Kinetic Energy Comparison – Analytical Mode 3 vs Test Mode 701

DOF	Analysis	Experimental
11	.08	.09
12	.31	.27
13	.00	.00
14	.00	.00
15	.00	.00
16	.00	.00
21	.20	.21
22	.06	.05
23	.00	.00
24	.00	.00
25	.00	.00
26	.00	.00
31	.05	.05
32	.05	.03
33	.00	.00
34	.00	.00
35	.00	.00
36	.00	.01
41	.00	.00
42	.06	.05

TABLE 15
Kinetic Energy Comparison – Analytical Mode 3 vs Test Mode 701 (contd)

DOF	Analysis	Experimental
43	.00	.00
44	.00	.00
45	.00	.00
46	.00	.00
51	.01	.01
52	.10	.08
53	.02	.01
54	.00	.00
55	.01	.00
56	.00	.00
61	.01	.01
62	.11	.07
63	.01	.01
64	.00	.00
65	.00	.00
66	.00	.01
71	.06	.08
72	.13	.14
73	.00	.01
74	.00	.00
75	.00	.01
76	.00	.01
81	.16	.14
82	.08	.06
83	.00	.00
84	.00	.00
85	.00	.00
86	.00	.01
91	.09	.08
92	.66	.62
93	.01	.01
94	.00	.00
95	.00	.00
96	.00	.00
101	.02	.02
102	.50	.54
103	.02	.00
104	.00	.00
105	.00	.00
106	.00	.00
111	.01	.01
112	.51	.42
113	.01	.00
114	.01	.00
115	.01	.02
116	.00	.00
121	.16	.11
122	.84	.84
123	.03	.01
124	.00	.00
125	.00	.06
126	.00	.05
131	.00	.00
132	1.02	.84
133	.02	.01
134	.00	.00
135	.00	.00
136	.00	.01
141	.12	.11

TABLE 15
Kinetic Energy Comparison – Analytical
Mode 3 vs Test Mode 701 (contd)

DOF	Analysis	Experimental
142	.35	.24
143	.00	.00
144	.00	.00
145	.00	.00
146	.00	.00
151	.02	.02
152	.39	.31
153	.00	.00
154	.00	.00
155	.00	.00
156	.00	.01
161	.00	.00
162	.51	.45
163	.00	.00
164	.00	.00
165	.00	.00
166	.01	.00
1011	5.39	4.75
1012	3.98	4.03
1013	.01	.02
1014	.43	.40
1015	7.59	6.56
1016	62.20	64.90
3011	4.55	4.10
3012	3.60	3.51
3013	.03	.01
3014	.02	.02
3015	.00	.00
3016	.11	.11
3031	2.63	2.34
3032	.33	.43
3033	.01	.02
3034	.02	.01
3035	.02	.03
3036	.10	.10
4011	.14	.12
4012	.00	.00
4013	.00	.00
4014	.00	.00

TABLE 15
Kinetic Energy Comparison – Analytical
Mode 3 vs Test Mode 701 (contd)

DOF	Analysis	Experimental
4015	.00	.00
4016	.03	.03
5011	.19	.18
5012	.04	.04
5013	.00	.00
5014	.00	.00
5015	.00	.00
5016	.02	.02
2011	.95	.78
2012	.06	.10
2013	.07	.03
2014	-.02	.02
2015	.24	.60
2016	-.03	.09
4021	.05	.05
4022	.00	.00
4023	.00	.00
4031	.05	.07
4032	.00	.00
4033	.00	.00
4041	.05	.05
4042	.00	.00
4043	.00	.00
6011	.02	.01
6012	.01	.01
6013	.00	.00
6021	.02	.02
6022	.10	.09
6023	.00	.00
6031	.01	.00
6032	.00	.00
6033	.00	.00
6041	.01	.01
6042	.07	.06
6043	.00	.00

RSS ERROR= .247+00

The local kinetic energy information is also valuable in identifying the mode shapes by describing the items with the largest kinetic energy. The data are also used in defining the system damping from the substructure damping measurements.

K. Modal Force

In the analysis, the modal forces of the truss members are calculated for each mode. During the test, strain gauge data were taken at these truss members from which the test modal forces are obtained. The calculated modal forces from the analysis and measured member forces from the test are compared.

Since the magnitudes of the analytical modal forces are arbitrary, a normalization factor is found to multiply the analytical value to make a meaningful comparison. This normalization factor is calculated as follows:

$$\alpha = \frac{\sum_{i=1}^{N} \left(P_i^A \, P_i^T \right)}{\sum_{i=1}^{N} \left(P_i^A \, P_i^A \right)} \qquad (39)$$

TABLE 16
Summary of Kinetic Energy Comparison

Mode / DOF		1	2	3	4	5	6
Bus (%)	A*	11.45	11.23	6.87	1.98	13.76	17.82
	T‡	11.38	11.43	6.25	1.54	11.90	14.41
Lander (%)	A	42.75	19.22	79.61	77.85	42.72	43.65
	T	40.58	21.88	80.65	77.35	44.25	42.51
Oxidizer tank (%)	A	25.64	39.35	8.32	11.16	23.81	21.05
	T	26.42	39.80	7.75	11.64	22.51	24.04
Fuel tank (%)	A	15.26	24.53	3.10	7.08	14.34	7.66
	T	16.01	21.22	2.93	7.52	15.46	9.18
Pressure tank (%)	A	0.84	0.79	0.18	0.05	0.23	0.73
	T	0.97	0.78	0.16	0.05	0.18	0.86
Engine (%)	A	0.93	2.00	0.25	1.02	1.31	0.84
	T	0.92	1.78	0.25	1.14	1.39	0.85
Scan platform (%)	A	2.08	1.92	1.27	0.64	3.22	7.30
	T	2.01	2.09	1.63	0.59	3.80	7.40
RSS (%)		0.452	0.319	0.247	0.208	0.233	0.330

*Analysis.
‡Test.

where

α = normalization factor

N = number of members

P_i^A = analytical modal force of the i^{th} member

P_i^T = test modal force of the i^{th} member

The factor α minimizes the difference between the analytical value and test value in the least-square sense. The analytical member forces are multiplied by α and compared with the test value. Table 17 shows this comparison together with the ratio of the comparison for a typical mode. The truss member identification is defined in Ref. (8). Only the axial forces are used in the comparison. The bending forces are not included in the comparison.

The discrepancies between the test and analysis are thought to be from two sources. One is the inherent disadvantage of using strain gauges that were setup for high strain reading from the static test. Since low levels of strain were recorded in the modal test, the accuracy of the reading is in question. The other source of discrepancy is the difference between the analysis and test mode shape. The modal forces are very sensitive to local differences in the mode shape.

TABLE 17
Axial Force Comparison – Factor = 6.076

Member	P (test) Mode 701 Freq = 7.840 Hz	P (analysis) Mode 3 Freq = 7.480 Hz	Ratio P (analysis) / P (test)
FEDFRAME			
BUS658	-.2319+02	-.2736+02	.1180+01
BUS660	.4773+01	.5832+01	.1222+01
BUS662	.2578+02	.3009+02	.1167+01
BUS664	-.9597+00	-.4137+01	.4311+01
SPACECRAFT TRUSS			
BUS686	-.4991+02	-.4710+02	.9437+00
BUS687	.1785+02	.1788+02	.1002+01
BUS688	.6892+02	.6239+02	.9052+00
BUS689	-.1110+03	-.1086+03	.9787+00
BUS690	-.5990+02	-.6524+02	.1089+01
BUS691	.2747+01	-.2310+01	-.8409+00
BUS692	-.1106+02	-.9632+01	.8709+00
BUS693	.6287+02	.6660+02	.1059+01
BUS694	.2033+03	.1998+03	.9806+00
BUS695	-.1613+03	-.1533+03	.9504+00
BUS696	-.1848+02	-.1939+02	.1049+01
BUS697	.6590+02	.5852+02	.8880+00
UPPER PLANE TRUSS			
BUS726	-.5537+02	-.4872+02	.8793+00
BUS727	.6018+02	.6321+02	.1050+01
BUS729	-.9699+01	-.1255+02	.1294+01
BUS730	-.2076+02	-.2627+02	.1265+01
BUS732	.7328+01	.9957+01	.1359+01
BUS742	.1023+03	.9305+02	.9096+00
BUS746	-.1085+03	-.9284+02	.8557+00
LANDER TRUSS			
BUS750	.1195+01	.6561+01	.5491+01
BUS751	-.1671+03	-.1615+03	.9667+00
BUS752	.9808+02	.9439+02	.9624+00
BUS753	-.1791+03	-.1794+03	.1001+01
BUS754	.2112+03	.2227+03	.1055+01
BUS755	.4500+02	.5093+02	.1130+01
BUS MAIN LONGERON			
BUS806	.3042+02	.3631+02	.1194+01
BUS810	.1692+02	.1527+02	.9079+00
BUS811	.5996+01	.1418+02	.2365+01
BUS813	-.1721+02	-.1518+02	.8823+00
BUS816	-.1381+03	-.1515+03	.1097+01
BUS818	-.1525+03	-.1313+03	.8611+00
BUS820	.4821+01	.5156+01	.1069+01
BUS823	-.1869+02	-.1806+02	.9663+00
BUS826	.2078+03	.2228+03	.1072+01
BUS830	.1413+00	-.9394+01	-.6648+02

TABLE 17
Axial Force Comparison – Factor = 6.076 (contd)

Member	P (test) Mode 701 Freq = 7.840 Hz	P (analysis) Mode 3 Freq = 7.480 Hz	Ratio P (analysis) / P (test)
BUS831	-.3867+02	-.3952+02	.1022+01
BUS832	.5098+02	.4784+02	.9384+00
BUS83E	-.1038+03	-.1059+03	.1020+01
BUS839	-.4313+01	-.1563+01	.3625+00
BUS84C	.1417+02	.1782+02	.1257+01
BUS841	-.2594+02	-.2123+02	.8184+00
PROPULSION SUBSYSTEM			
PPP003	.7637+01	.3336+01	.4369+00
PPP004	-.5652+01	.9120+01	-.1614+01
PPP008	.8962+01	.1566+02	.1747+01
PPP011	.1276+02	.1552+02	.1216+01
PPP012	-.6829+02	-.6563+02	.9610+00
PPP019	-.1608+01	-.1349+02	.8391+01
PPP028	.9454+00	.2603+01	.2753+01
PPP036	.5470+02	.4360+02	.7970+00
PPP037	.2029+02	.8557+01	.4217+00
PPP04C	-.2429+02	-.2961+02	.1219+01
PPP041	.1826+02	.2142+02	.1173+01
PPP043	.5946+01	.6036+01	.1015+01
PPP057	-.5330+01	-.3619+01	.6790+00
PPP082	.2706+00	-.2533+01	-.9361+01
R.S.S. ERROR OF TEST VS ANALYSIS COMPARISON OF AXIAL FORCES			
		NORMALIZATION FACTOR	RSS ERROR OF FORCES
INPUT FACTOR		.000	.000
CALCULATED FACTOR		6.076	6.937
C.E.=	.5462+00		
W.E.=	.1682+00		

Several methods are used to establish a measure of error. They are:

Description	Relation	Reason
Least square error (LSE)	$\left[\frac{1}{N}\sum_{i=1}^{N}\left(P_i^T - P_i^A\right)^2\right]^{1/2}$	No weight

Description	Relation	Reason
Weighted least square error (WLSE)	$\left[\frac{1}{N}\sum_{i=1}^{N}\left(\frac{\epsilon_T}{\epsilon_{FS}}\right)\left(P_i^T - P_i^A\right)^2\right]^{1/2}$	Weighted readings with higher strain
Composite error (CE)	$\left[\frac{\sum_{i=1}^{N}\left\|P_i^T\right\|\left[\frac{P_i^T - P_i^A}{P_i^A}\right]^2}{\sum_{i=1}^{N}\left\|P_i^T\right\|}\right]^{1/2}$	Weighted readings with higher forces

where

ϵ_T = test strain gauge reading

ϵ_{FS} = full scale strain gauge reading

The results of the various weighting methods are in Table 18. Also the composite error is applied only to the Viking lander capsule adapter (VLCA) and V-S/C-A as shown in Table 19 to compare the data with the proof launch spacecraft Modal test (Ref. 9).

TABLE 18
Modal Force Comparison Errors

Mode		Least Square Error (lb)	Weighted Least Square Error (lb)	Composite Error (%)
Analysis	Test			
1	708	53.01	2.09	74.82
2	703	32.28	0.90	50.62
3	701	6.94	0.94	54.62
4	702	17.69	0.030	19.40
5	704	9.19	0.015	19.89
6	705	6.38	0.086	21.94
7	711	28.41	1.16	35.54
8	717	42.66	1.37	75.13
9	712	45.87	1.73	72.12
10	707	2.26	0.0035	51.87
11	714	22.39	0.29	101.3
12	713	52.71	1.61	98.83

TABLE 19
Composite Error of VLCA and V-S/C-A

Mode		VLCA (%)	V-S/C-A (%)
Analysis	Test		
1	708	55.75	46.81
2	703	54.56	41.67
3	701	18.81	12.06
4	702	5.37	7.19
5	704	8.20	17.52
6	705	25.46	8.53
7	711	21.82	14.89
8	717	49.18	51.88
9	712	79.37	82.52
10	707	29.95	59.40
11	714	102.0	108.6
12	713	62.99	21.99

To help resolve the source of discrepancy, test force coefficients are checked using the modal acceleration data. The truss loads resulting from the modal acceleration times the mass applied as a static load are compared to the modal force coefficient. The comparison for the VLCA members is shown in Table 20. The good correlation indicates the error to be the result of the difference in the analytical and test modes.

TABLE 20
Comparison of Modal Force by Inertia Load – Mode 713, Frequency 26.49 Hz

Member No.	Test (lb)	Inertia (lb)	Analysis (lb)
750	161	175	134
751	53	47	-20
752	262	299	166
753	279	291	290
754	116	131	-44
755	104	130	157
LSE		20.92	85.41
CE		12.76	62.99

Future efforts will be to obtain the force coefficient throughout the structure by application of the modal acceleration times the mass as an external load.

L. Strain Energy

Strain energy (SE) of a mode is a significant parameter in the description of a mode shape, especially when modal forces are of interest. Equation (5) directly relates strain energy to the stiffness matrix.

For a mode, strain energy values describe the member or sets of members with the largest forces and deformations whereas kinetic energy (KE) describes the masses with the largest inertial motion. The significant difference is the SE of the system is directly related to relative displacements at the ends of the members whereas KE is directly related to the absolute displacement.

The axial strain energy of the i^{th} member monitored during the modal test is

$$(SE)_i = \frac{1}{2} \frac{F_i^2 L_i}{A_i E_i} \tag{40}$$

where

$(SE)_i$ = strain energy of the i^{th} member

F_i = force in the i^{th} member

L_i = length of the i^{th} member

A_i = cross-sectional area of the i^{th} member

E_i = modulus of elasticity of the i^{th} member

The SE of each axial member for both analysis and test is listed in the order of its magnitude. Also the SE of each member group is listed to help identify the characteristics of the mode shape. Table 21 shows the strain energy of each member and the comparison between test and analysis of a typical mode both in its magnitude and percentage. Table 22 shows the comparison of the same mode listed in the order of magnitude. Table 23 shows the percentage SE of each member group for the first twelve modes.

TABLE 21
Strain Energy Comparison – Analytical Mode 3 vs Test Mode 701

Member	Test (in.-lb)	Analysis (in.-lb)	Test (%)	Analysis (%)
SEDFRAME				
BUS659	.4564-02	.6497-02	.2716-02	.3875-02
BUS660	.2770-03	.4145-03	.1616-03	.2472-03
BUS662	.5656-02	.7705-02	.3294-02	.4596-02
BUS664	.1118-04	.2078-03	.6511-05	.1239-07
TOTAL=	.1061-01	.1482-01	.6178-02	.8842-02
SPACECRAFT TRUSS				
BUS685	.1435-01	.1278-01	.8355-02	.7621-02
BUS687	.2637-02	.2646-02	.1536-02	.1578-02
BUS688	.3074-01	.2519-01	.1790-01	.1503-01
BUS689	.7540-01	.7318-01	.4449-01	.4365-01
BUS690	.3551-01	.4213-01	.2068-01	.2513-01
BUS691	.4128-04	.2919-04	.2404-04	.1741-04
BUS692	.6694-03	.5077-03	.3898-03	.3028-03
BUS693	.3192-01	.3582-01	.1859-01	.2136-01
BUS694	.2507+00	.2410+00	.1460+00	.1438+00
BUS695	.1548+00	.1397+00	.9003-01	.8330-01
BUS696	.3365-02	.3705-02	.1960-02	.2210-02
BUS697	.2347-01	.1351-01	.1367-01	.1104-01
TOTAL=	.6244+00	.5952+00	.3636+00	.3550+00
UPPER PLANE TRUSS				
BUS726	.9999-02	.7741-02	.5822-02	.4617-02
BUS727	.1133-01	.1251-01	.6600-02	.7459-02
BUS728	.2151-03	.3603-03	.1253-03	.2149-03
BUS730	.1613-02	.2583-02	.9393-03	.1541-02
BUS732	.1239-03	.2285-03	.7208-04	.1363-03
BUS742	.8196-01	.6781-01	.4773-01	.4045-01
BUS746	.1056+00	.7729-01	.6147-01	.4610-01
TOTAL=	.2108+00	.1685+00	.1228+00	.1005+00
LANDER TRUSS				
BUS750	.1083-04	.3266-03	.6309-05	.1948-03
BUS751	.2261+00	.2113+00	.1317+00	.1260+00
BUS752	.5158-01	.4777-01	.3004-01	.2850-01
BUS753	.1608+00	.1613+00	.9365-01	.9619-01
BUS754	.3613+00	.4019+00	.2104+00	.2397+00
BUS755	.1647-01	.2101-01	.9592-02	.1253-01
TOTAL=	.9163+00	.8435+00	.4753+00	.5031+00
BUS MAIN LONGERON				
BUS808	.2185-03	.3113-03	.1272-03	.1857-03
BUS810	.4136-03	.3408-03	.2409-03	.2033-03
BUS811	.1788-04	.9997-04	.1041-04	.5963-04
BUS813	.5177-03	.4030-03	.3015-03	.2404-03
BUS816	.4413-02	.5312-02	.2570-02	.3169-02
BUS819	.5389-02	.3995-02	.3138-02	.2383-02
BUS820	.3215-04	.3677-04	.1872-04	.2193-04
BUS823	.6257-03	.5843-03	.3644-03	.3485-03
BUS826	.1037-01	.1187-01	.6015-02	.7081-02

TABLE 21
Strain Energy Comparison – Analytical Mode 3 vs Test Mode 701 (contd)

Member	Test (in.-lb)	Analysis (in.-lb)	Test (%)	Analysis (%)
BUS830	.3011-07	.1331-03	.1753-07	.7937-04
BUS831	.3941-02	.4116-02	.2295-02	.2455-02
BUS832	.4839-02	.4262-02	.2818-02	.2542-02
BUS83[illegible]	.2548-02	.2650-02	.1483-02	.1581-02
BUS839	.2664-04	.3500-05	.1551-04	.2088-05
BUS840	.4802-03	.7590-03	.2796-03	.4527-03
BUS841	.1170-02	.7835-03	.6812-03	.4673-03
TOTAL=	.3498-01	.3566-01	.2036-01	.2127-01
PROPULSION SUBSYSTEM				
PPP003	.1049-03	.2002-04	.6109-04	.1194-04
PPP004	.6654-04	.1733-03	.3875-04	.1034-03
PPP009	.4594-03	.1402-02	.2675-03	.8363-03
PPP011	.3571-03	.5280-03	.2080-03	.3149-03
PPP012	.9433-02	.8711-02	.5493-02	.5196-02
PPP018	.8424-05	.5931-03	.4906-05	.3538-03
PPP029	.2150-05	.1630-04	.1252-05	.9721-05
PPP036	.6633-02	.4213-02	.3863-02	.2513-02
PPP037	.7946-03	.1413-03	.4627-03	.8430-04
PPP040	.1057-02	.1570-02	.6154-03	.9365-03
PPP041	.7524-03	.1036-02	.4382-03	.6177-03
PPP047	.2831-03	.2917-03	.1648-03	.1740-03
PPP053	.2287-03	.1054-03	.1332-03	.6289-04
PPP082	.2134-06	.1870-04	.1243-06	.1115-04
TOTAL=	.2019-01	.1882-01	.1175-01	.1123-01
TOTAL=	.1717+01	.1677+01	.1000+01	.1000+01

R.S.S. ERROR OF TEST VS ANALYSIS COMPARISON OF STRAIN ENERGY

	NORMALIZATION FACTOR	RSS ERROR OF FORCES
INPUT FACTOR	6.076	6.937
CALCULATED FACTOR	.933	.001

TABLE 22
Strain Energy in Order of Magnitude – Analytical Mode 3 vs Test Mode 701

Member	Strain Energy (Test) (in.-lb)	Member	Strain Energy (Analysis) (in.-lb)
BUS754	.2104+00	BUS754	.2397+00
BUS694	.1460+00	BUS694	.1438+00
BUS751	.1317+00	BUS751	.1260+00
BUS753	.9365-01	BUS753	.9619-01
BUS695	.9003-01	BUS695	.8330-01
BUS746	.6147-01	BUS746	.4610-01
BUS742	.4773-01	BUS689	.4365-01
BUS689	.4449-01	BUS742	.4045-01
BUS752	.3004-01	BUS752	.2850-01
BUS690	.2068-01	BUS690	.2513-01

TABLE 22
Strain Energy in Order of Magnitude – Analytical Mode 3 vs Test Mode 701 (contd)

Member	Strain Energy (Test) (in.-lb)	Member	Strain Energy (Analysis) (in.-lb)
BUS693	.1859-01	BUS693	.2136-01
BUS688	.1790-01	BUS688	.1503-01
BUS697	.1367-01	BUS755	.1253-01
BUS755	.9592-02	BUS697	.1104-01
BUS686	.8355-02	BUS695	.7621-02
BUS727	.6600-02	BUS727	.7459-02
BUS925	.6015-02	BUS825	.7081-02
BUS720	.5922-02	PPP012	.5196-02
PPP012	.5493-02	BUS725	.4617-02
PPP036	.3863-02	BUS662	.4596-02
BUS662	.3294-02	BUS553	.3375-02
BUS818	.3138-02	BUS816	.3169-02
BUS832	.2818-02	BUS832	.2542-02
BUS658	.2716-02	PPP036	.2513-02
BUS816	.2570-02	BUS831	.2455-02
BUS831	.2295-02	BUS818	.2383-02
BUS695	.1960-02	BUS696	.2210-02
BUS687	.1536-02	BUS835	.1581-02
BUS835	.1483-02	BUS687	.1578-02
BUS730	.9393-03	BUS730	.1541-02
BUS841	.6812-03	PPP040	.9365-03
PPP040	.6154-03	PPP008	.8363-03
PPP037	.4627-03	PPP041	.6177-03
PPP041	.4382-03	BUS841	.4673-03
BUS692	.3898-03	BUS840	.4527-03
BUS823	.3644-03	PPP018	.3538-03
BUS813	.3015-03	BUS823	.3485-03
BUS840	.2796-03	PPP011	.3149-03
PPP008	.2575-03	BUS692	.3028-03
BUS810	.2409-03	BUS660	.2472-03
PPP011	.2080-03	BUS813	.2404-03
PPP042	.1648-03	BUS728	.2149-03
BUS660	.1616-03	BUS810	.2033-03
PPP053	.1332-03	BUS750	.1948-03
BUS906	.1272-03	BUS806	.1957-03
BUS728	.1253-03	PPP043	.1740-03
BUS732	.7209-04	BUS732	.1363-03
PPP003	.6109-04	BUS664	.1239-03
PPP004	.3975-04	PPP004	.1034-03
BUS691	.2404-04	PPP037	.8430-04

M. Reaction Forces

The calculation of reaction forces at the base of the VTA/CTA by the modal forces from the V-S/C-A strain gages and the modal accelerations provides a check on the test data.

The $[\overline{M}^{RE}]_T$ matrix from Eq. (30d) represents the reaction forces from the modal accelerations. The reaction forces calculated from the V-S/C-A modal member force data are compared to $[\overline{M}^{RE}]_T$. The comparison of the data are in Table 24.

N. Generalized Mass from Modal Damping

The generalized mass terms $\left[\overline{M}^{EE}\right]$ from Eq. (30d) are checked by the following relationship. At a normal mode, the damping values are offset by the force values. From Eq. (28),

$$[\overline{C}]_T\{\dot{q}\}_T = [\Phi]_T^T\{f\}_T \qquad (41)$$

for the n^{th} mode. Since

TABLE 23
Strain Energy Distribution Comparison

Mode		Bedframe (%)	V-S/C Truss (%)	Upper Plane Truss (%)	Lander Truss (%)	Bus Main Longeron (%)	Propulsion Subsystem (%)
1	A*	0.01	0.86	0.03	0.09	0.04	0.02
	T‡	0.01	0.84	0.03	0.08	0.04	0.03
2	A	0.09	0.73	0.03	0.04	0.01	0.10
	T	0.06	0.78	0.02	0.04	0.01	0.09
3	A	0.09	0.36	0.10	0.50	0.02	0.01
	T	0.06	0.36	0.12	0.48	0.02	0.01
4	A	0.10	0.35	0.03	0.42	0.04	0.06
	T	0.07	0.40	0.03	0.40	0.04	0.06
5	A	0.0	0.54	0.03	0.30	0.04	0.09
	T	0.0	0.55	0.04	0.26	0.04	0.12
6	A	0.05	0.43	0.05	0.31	0.04	0.13
	T	0.04	0.47	0.07	0.24	0.04	0.15
7	A	0.26	0.22	0.05	0.11	0.06	0.35
	T	0.20	0.24	0.08	0.11	0.07	0.38
8	A	0.36	0.09	0.01	0.09	0.02	0.44
	T	0.26	0.11	0.02	0.25	0.03	0.34
9	A	0.20	0.05	0.05	0.44	0.03	0.23
	T	0.20	0.05	0.04	0.38	0.04	0.29
10	A	0.01	0.08	0.02	0.57	0.02	0.30
	T	0.04	0.07	0.02	0.58	0.03	0.28
11	A	0.10	0.22	0.06	0.46	0.02	0.13
	T	0.04	0.22	0.27	0.58	0.01	0.08
12	A	0.06	0.08	0.10	0.63	0.02	0.11
	T	0.10	0.23	0.03	0.51	0.03	0.12

*Analysis.

‡Test.

TABLE 24
Comparison of Reaction Force

Mode	Reaction Force: Accelerometer (Strain Gage)[a]					
	F_X (lb)	F_Y (lb)	F_Z (lb)	M_X (in.-lb)	M_Y (in.-lb)	M_Z (in.-lb)
708	401 (517)	-120 (-169)	-8 (54)	16700 (15587)	60000 (52441)	-1270 (-1565)
703	75 (78)	383 (391)	8 (-102)	-52400 (-33728)	11600 (6802)	1394 (1926)
701	45 (50)	-28 (-36)	-4 (-10)	10300 (9540)	1110 (-1398)	11400 (12847)
702	19 (14)	131 (138)	19 (-22)	-49300 (-44093)	59 (-1311)	2440 (2374)
704	-2 (-1)	19 (-1)	-44 (-50)	-3900 (-1585)	23700 (25842)	8060 (9087)
705	25 (22)	-4 (5)	-107 (-119)	684 (62)	15000 (14108)	-3440 (-4483)
711	12 (5)	-2 (-2)	1080 (1106)	241 (974)	18100 (18207)	-2240 (-3388)
717	17 (28)	-6 (-40)	444 (465)	1810 (3392)	833 (762)	-1490 (-557)
712	2 (17)	28 (81)	125 (97)	2600 (-6375)	-438 (248)	1200 (920)

[a]Numbers in parentheses refer to strain gage measurements.

$$\bar{C}_{nn} = 2\rho_n \bar{M}_{nn} \omega_n \qquad (42)$$

then

$$\bar{M}_{nn} = \frac{\left\lfloor \Phi_{ij} \right\rfloor}{2\rho_n \omega_n \dot{q}_n} \left\{ f \right\} \qquad (43)$$

Each generalized mass term $\bar{M}_{nn}$ is calculated from Eq. (43) by measuring the modal damping, frequency, velocity of the participation factor, shaker force, and displacement in the force direction. The comparison is in Table 25. Since the modal damping ρ_n varied, the $\bar{M}_{nn}$ varied accordingly. As noted, the $\bar{M}_{nn}$ is within the range of the damping measured; however, because of the variation in ρ_n, $\bar{M}_{nn}$ cannot be accurately measured by this method.

TABLE 25
Generalized Mass Comparison

Mode	Based on Damping			Based on Mode Shape
	High	Aver-age	Low	
708	0.065	0.141	1.021	0.261
703	0.111	0.179	0.617	0.252
701	0.130	0.227	0.833	0.290
702	0.063	0.091	0.410	0.364
704	0.133	0.290	0.785	0.344
705	0.056	0.081	0.330	0.244
711	0.902	1.499	3.037	0.881
712	1.111	2.043	5.557	0.776
707	0.011	0.024	0.060	0.083
714	0.171	0.376	3.141	0.397
713	1.292	2.179	6.692	1.101

FINAL DYNAMIC MODEL

The final VO dynamic model is a combination of the modal test configuration and substructure characteristics verified by substructure tests. Since Eq. (22) representing the modal test configuration was verified by test, the parameters are accurate. Modifications are made to update the parameters to the V-S/C Mission B configuration. The subscript FB denotes Mission B configuration. The changes are:

CHANGES	REASON
$[M]_{T,A}$ to $[M]_{FB}$	The mass of the propellant is changed to the Mission B configuration; see Table 2.
$\{q\}_{P,T}$ to $\{q\}_{P,FB}$	The dynamic characteristics of the propulsion module changes
$\{q\}_{S,T}$ to $\{q\}_{S,FB}$	The dynamic characteristic of the scan platform changes since its joint is allowed to move along the serrations

The parameters verified by the modal test and updated to represent Mission B are combined with the remainder of the substructures. Each substructure is verified by a modal test. The combined equation of motion represented by Eq. (18) becomes

$$[M]_{FB}\begin{Bmatrix} \{\ddot{u}\}_R \\ \{\ddot{u}\}_B \\ \{\ddot{q}\}_P \\ \{\ddot{q}\}_S \\ \{\ddot{q}\}_C \\ \{\ddot{q}\}_{SPA} \\ \{\ddot{q}\}_{SP1} \\ \{\ddot{q}\}_{SP2} \\ \{\ddot{q}\}_{SP3} \end{Bmatrix}_{FB} + [C]_{FB}\begin{Bmatrix} \{\dot{u}\}_R \\ \{\dot{u}\}_B \\ \{\dot{q}\}_P \\ \{\dot{q}\}_S \\ \{\dot{q}\}_C \\ \{\dot{q}\}_{SPA} \\ \{\dot{q}\}_{SP1} \\ \{\dot{q}\}_{SP2} \\ \{\dot{q}\}_{SP3} \end{Bmatrix}_{FB} + [K]_{FB}\begin{Bmatrix} \{u\}_R \\ \{u\}_B \\ \{q\}_P \\ \{q\}_S \\ \{q\}_C \\ \{q\}_{SPA} \\ \{q\}_{SP1} \\ \{q\}_{SP2} \\ \{q\}_{SP3} \end{Bmatrix}_{FB} = [0] \tag{44}$$

$$\{P\}_B = [S]\{u\}_B \tag{45}$$

$$\{P\}_i = [S][\phi]_i\{u\}_i \tag{46}$$

Table (26) summarizes the various parameters verified by the corresponding tests.

TABLE 26
Test Verified Models

Parameter	Description	Test for Verification
$[M]_{FB}$	Mission B mass matrix	All the modal tests and the propellant effective weight tests
$\{U_R\}$	Rigid body mode	Calculations $\bar{M}_{FB}^{RR}$ should check with the rigid inertia properties of the V-S/C/CTA/CTA at its base
$\{U_B\}$	Model of bus with CTA/VTA	Static test on the bus and system modal test; the CTA/VTA only included in the system modal test
$\{q\}_P$	Displacement function of propulsion	Modal and static test of propulsion module and system modal test with referee fluid
$\{q\}_S$	Displacement function of scan platform	Modal Test of scan platform and system modal test without joint slippage; the joint slippage was included for load analysis since higher forces would result in joint slippage
$\{q\}_C$	Displacement function of cable trough	Modal Test of cable trough and system modal test
$\{q\}_{SPA}$	Displacement function of solar panel with relay antenna	Modal and static solar panel tests with a relay antenna
$\{q\}_{SPi}$ $(i = 1, 3)$	Displacement function of solar panel	Based upon a mathematical model of the solar panel with a relay antenna; the relay antenna was removed from the math model for this configuration
$[C]_{FB}$	Damping matrix for Mission B configuration	Data based upon modal tests where available; the damping matrix was diagonalized at each transformation; the kinetic energy evaluation of the modes was used as a guide to estimate damping; solar panel viscous dampers were not included but estimated as a modal damping
$[K]_{FB}$	Stiffness matrix for Mission B configuration	Substructure modal and static tests; system modal tests
$[S]$	Load matrix	Substructure modal and static tests; system modal tests

The real eigenvalues and eigenvectors of Eq. (44) with $[C]_{FB} = 0$, results in

$$\begin{Bmatrix} \{u\}_R \\ \{u\}_B \\ \{q\}_P \\ \{q\}_S \\ \{q\}_C \\ \{q\}_{SPA} \\ \{q\}_{SP1} \\ \{q\}_{SP2} \\ \{q\}_{SP3} \end{Bmatrix}_{FB} = [\Phi]_{FB} \begin{Bmatrix} \{u\}_R \\ \{X\}_{FB} \end{Bmatrix} \tag{47}$$

Substitution of Eq. (47) with Eq. (44) and premultiplication of $[\Phi]^T_{FB}$ results in

$$\begin{bmatrix} M^{RR}_{FB} & M^{RE}_{FB} \\ M^{ER}_{FB} & \left[M^{EE}_{FB}\right] \end{bmatrix} \begin{Bmatrix} \{\ddot{u}\}_R \\ \{\ddot{X}\}_{FB} \end{Bmatrix} + \begin{bmatrix} 0 & 0 \\ 0 & \left[C^{EE}_{FB}\right] \end{bmatrix} \begin{Bmatrix} \{\dot{u}\}_R \\ \{\dot{X}\}_{FB} \end{Bmatrix} + \begin{bmatrix} 0 & 0 \\ 0 & \left[K^{EE}_{FB}\right] \end{bmatrix} \begin{Bmatrix} \{u\}_R \\ \{X\}_{FB} \end{Bmatrix} = [0] \tag{48}$$

$$\{P\}_B = [S][\Phi]_{FB}\{X\}_{FB} \tag{49}$$

$$\{P\}_i = [S][\Phi]_i [\Phi]_{FB}\{X\}_{FB} \tag{50}$$

The procedure to obtain the flight model was not complicated. The effort required to obtain $\left[C^{EE}_{FB}\right]$ was based upon engineering judgement. Since damping for most substructures is measured or estimated, the system damping matrix was based upon the kinetic energy contribution of the substructures to the system mode.

The data represented by Eqs. (48) through (50) was transmitted to MMA to couple the VLC on the VO to obtain the V-S/C mathematical model.

CONCLUSION

Highlights of the steps leading to the VO dynamic model are summarized with the mathematical equations and data. The success is attributed to substructure modal coupling concepts where each substructure is experimentally verified. The degree of correlation is dependent on the use of the dynamic model. The mode shapes and frequencies of the system correlated well but some difficulty exists in correlating modal forces. A measure to establish the degree of correlation is still required.

An overall structures and dynamics program integrating the substructure analysis, hardware availability, and test will result in a successful dynamic model. Overall system modal tests may not be required.

REFERENCES

1. W. C. Hurty, Dynamic Analyses of Structural Systems by Component Mode Synthesis, Technical Report 32-530. Jet Propulsion Laboratory, Pasadena, California, January 1964.
2. L. Leppert, R. Miyakawa, and B. Wada, "Modal Test Results of the Viking Orbiter," paper presented at the 44th Shock and Vibration Symposium, Dec. 4-7, 1973, Houston, Texas.
3. B. K. Wada, "Viking Orbiter-Dynamics Overview," paper presented at the 44th Shock and Vibration Symposium, Dec. 4-7, 1973, Houston, Texas.

4. W. A. Benfield and R. F. Hruda, "Vibration Analyses of Structures by Component Mode Substitution," presented at AIAA/ASME 11th Structures, Structural Dynamics, and Materials Conference, Denver, Colorado, April 22-24, 1970. Also published in AIAA J. Vol. 9, No. 7, July 1971, pp. 1255-1261.

5. R. M. Bamford, A Modal Combination Program for Dynamic Analysis of Structures, Technical Memorandum 33-290. Jet Propulsion Laboratory, Pasadena, California, August 1966.

6. R. Bamford, B. K. Wada, J. A. Garba, and J. Chisholm, "Dynamic Analysis of Large Structural Systems," presented at the Winter Annual Meeting of the ASME, Washington, D.C., Nov. 30, 1971. Also published in Synthesis of Vibrating Systems, ASME, New York, 1971, pp. 57-71.

7. R. M. Bamford, B. K. Wada, and W. H. Gayman, Equivalent Spring-Mass System for Normal Modes, Technical Memorandum 33-380. Jet Propulsion Laboratory, Pasadena, California, February 1971.

8. E. Leppert, "VO'75 Test Plan, ODTM with VTA/CTA Modal Test," Project Document 611-59. Jet Propulsion Laboratory, Pasadena, California, May 9, 1973 (JPL internal document).

9. A. Leondis, "Viking Dynamic Simulator Modal Test Report," SD-73-096. General Dynamics/Convair Astronautics, San Diego, Calif., August 31, 1973.

NASA—JPL—Coml., L. A. Calif.